

Infinite-component BF topological field theory: Nexus of fracton order, Toeplitz braiding, and non-Hermitian Amplification

Bo-Xi Li and Peng Ye^{ID*}

School of Physics, State Key Laboratory of Optoelectronic Materials and Technologies, and Guangdong Provincial Key Laboratory of Magnetoelectric Physics and Devices, Sun Yat-sen University, Guangzhou, 510275, China

(Dated: Wednesday 14th January, 2026)

Building on the infinite-component Chern–Simons theory of three-dimensional fracton phases by Ma *et al.* [Phys. Rev. B **105**, 195124 (2022)] and the Toeplitz braiding of anyons by Li *et al.* [Phys. Rev. B **110**, 205108 (2024)], we show that stacking (3 + 1)D BF topological field theories along a fourth spatial direction gives rise to an exotic class of four-dimensional fracton phases. Their low-energy physics is governed by a new field-theoretic framework—*infinite-component BF* (iBF) theories—characterized by asymmetric integer Toeplitz K matrices. Under open boundary conditions, iBF theories exhibit a striking phenomenon: *Toeplitz particle–loop braiding*, where a particle and a loop placed on opposite three-dimensional boundaries acquire a finite braiding phase even at infinite separation. This nonlocal braiding admits a geometric interpretation: transporting the particle induces a winding boundary trajectory on the opposite boundary that encircles the loop. We show that this robustness originates from boundary zero singular modes (ZSMs) of Toeplitz K matrices revealed by singular value decomposition (SVD), rather than from the eigenvalue zero modes responsible for previously known Toeplitz braiding of anyons. We analytically and numerically study representative iBF theories with Hatano–Nelson–type and non-Hermitian Su–Schrieffer–Heeger–type K matrices, establishing a universal correspondence between ZSMs and Toeplitz particle–loop braiding. Our results identify boundary zero singular modes as the mechanism behind Toeplitz particle–loop braiding and establish infinite-component BF theory as a predictive framework for higher-dimensional fracton topological orders.

CONTENTS

| | | | |
|---|----|--|----|
| I. Introduction | 1 | D. Equivalence Between Eigendecomposition and SVD in Capturing Toeplitz Braiding for Symmetric K matrix | 14 |
| A. Infinite-component Chern–Simons theory, anyonic Toeplitz braiding, and topological edge states | 1 | V. Conclusion and outlook | 15 |
| B. Infinite-component BF field theory, particle–loop Toeplitz braiding and boundary zero singular modes | 2 | Acknowledgments | 15 |
| II. Braiding in iBF theories | 4 | A. Detailed calculation on ZSMs | 15 |
| A. Multi-component BF theories | 4 | 1. Detailed calculation on ZSMs of HN-type K matrices | 15 |
| B. Construction of infinite-component BF theories | 5 | 2. Detailed calculation on ZSMs of nSSH-type K matrices | 16 |
| III. iBF theory with Hatano–Nelson type K matrix | 6 | References | 18 |
| A. Toeplitz braiding and ZSMs—a concrete example | 6 | | |
| B. General theory of Toeplitz braiding and ZSMs | 7 | I. INTRODUCTION | |
| C. Numerical results | 8 | | |
| IV. iBF theory with non-Hermitian Su–Schrieffer–Heeger type K matrix | 10 | A. Infinite-component Chern–Simons theory, anyonic Toeplitz braiding, and topological edge states | |
| A. Toeplitz Braiding encoded in Su–Schrieffer–Heeger type K matrix | 10 | Recently, <i>fracton topological order</i> (FTO) has emerged as a distinctive frontier in quantum many-body systems [1–5], driving advances in condensed matter and quantum physics [6–20]. Solvable realizations of FTO, known as fracton codes, include the 3d ¹ X-cube model | |
| B. ZSMs and Toeplitz braiding | 11 | | |
| C. Numerical results | 12 | | |

* yepeng5@mail.sysu.edu.cn

¹ In this paper, “ $(n + 1)D$ ” refers to $(n + 1)$ -dimensional spacetime with n -dimensional real space. We avoid using “ nD ” or “ $(n)D$ ”

and Haah's code [3–5]. In arbitrary dimensions, generalizations called “tetradigit stabilizer codes” have been proposed [13–16]. Their excitations—collectively referred to as *fractonic excitations*—exhibit restricted mobility: point-like fractons are immobile, lineons move only along lines, and planeons are confined to planes. This sharply contrasts with liquid-like topological orders such as the toric code, where anyons propagate freely via string operators. Studies of FTO have further inspired subsystem symmetry-protected topological phases [21–33] and many-body systems with conserved multipole moments [34–36]. The former generalize global symmetries to lower-dimensional subsystems; the latter impose strong kinematic constraints, yielding unconventional quantum phenomena [37–95].

A large subclass of FTOs exhibits a foliation structure, allowing them to be viewed as stacks of coupled 2d topological orders. This perspective provides a natural route to field-theoretical descriptions of fracton phases. Recent studies have developed stacking-based continuum or effective field theories [96–110]. Among these, the infinite-component Chern–Simons (iCS) theory—constructed by stacking multi-component Chern–Simons layers—has proven particularly promising [103–110]. Before proceeding, we briefly recall the basic structure of the (2+1)D multi-component Chern–Simons theory, which serves as a prototypical topological field theory capturing the low-energy physics of Abelian topological orders.

In (2+1)D multi-component Chern–Simons theory, topological quantities such as braiding statistics, ground-state degeneracy on a torus, and chiral central charge are encoded in the symmetric integer K matrix [111, 112]. This framework covers many topologically ordered phases, including multilayer fractional quantum Hall states and certain spin liquids [112]. It also provides a systematic method for classifying symmetry-enriched (SET) and symmetry-protected (SPT) phases in 2d [113–119]. The Abelian Chern–Simons theory considered here follows a hydrodynamical approach, distinct from the flux-attachment formulation [120–123].

To construct 3d FTOs, we treat each 2d (xy plane) Abelian topological order described by (2+1)D multi-component Chern–Simons theory as a 2d “layer” and stack them along the z direction, coupling adjacent layers via additional Chern–Simons terms that preserve translational invariance. This yields a multi-component Chern–Simons theory whose topological data are encoded in a symmetric integer block-Toeplitz (K) matrix [110, 124].

The action of such a theory is

$$S = \int \frac{K_{I,J}}{4\pi} a^I \wedge da^J, \quad K = \begin{pmatrix} A & B^\top \\ B & A & B^\top \\ & B & A & B^\top \\ & & \ddots & \ddots & \ddots \\ & & & B & A & B^\top \\ & & & & B & A \end{pmatrix}. \quad (1)$$

Here $a^{I,J}$ ($I, J = 1, \dots, N$) are $U(1)$ compact gauge fields, and implicit summation is assumed over these indices, which also label positions along z . The absence of lower-left and upper-right blocks in K indicates open boundary conditions (OBC) along the stacking direction. In the limit $N \rightarrow \infty$, this construction yields the infinite-component Chern–Simons (iCS) theory. The system boundaries fall into two classes: the xy surfaces of each layer and the z boundaries along the stacking direction. While the xy boundaries are conventional and can be described by stacked conformal field theories, the novel z boundaries were only understood after the discovery of Toeplitz braiding in Ref. [110].

Specifically, under OBC in the z direction, boundary zero modes of the K matrix, together with noninteger elements in the upper-right and lower-left corners of K^{-1} , generate nonlocal braiding statistics between particles on opposite z boundaries. Such exotic braiding statistics is demonstrated in Figs. 5 and 6 of Ref. [110]. This phenomenon, termed “Toeplitz braiding”, reveals a mathematical structure closely resembling the boundary theory of topological insulators and superconductors in free-fermion systems [125], establishing a link between strongly and weakly correlated systems.

B. Infinite-component BF field theory, particle-loop Toeplitz braiding and boundary zero singular modes

Building on the above iCS framework and the concept of Toeplitz braiding between anyons, this work takes a further step by extending the stacking construction from 2d to 3d topological orders, thereby realizing 4d FTOs. Our primary goal is to explore the resulting Toeplitz braiding between particles and loops within this higher-dimensional framework, as shown in Fig. 1. In contrast to conventional particle–loop linking processes in three dimensions, the braiding phases uncovered here arise from boundary-induced geometric winding and are intrinsically nonlocal along the stacking direction. As shown in Fig. 1, although the particle and the loop reside on opposite (3+1)D boundaries and may be separated by an arbitrarily large distance along the stacking (w) direction, adiabatically transporting the particle does not remain invisible to the loop. Instead, due to the interlayer BF couplings (to be introduced shortly), the motion of the particle induces an effective boundary trajectory on the opposite boundary, depicted by the blue path

unless otherwise specified. When referring specifically to spatial dimensions, we use “nd”, e.g., 3d ground state, 3d topological order, 3d cubic lattice and 1d closed string.

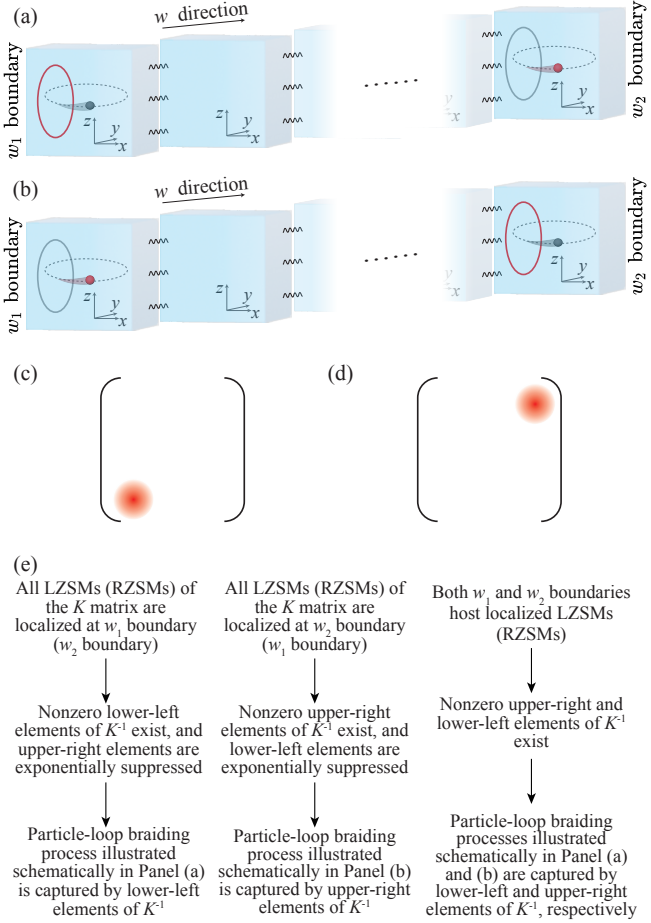


FIG. 1. Illustration of stacking and Toeplitz particle-loop braiding in iBF theories. Each so-called “layer” is a genuine three-dimensional *BF* theory defined on a three-torus and is schematically represented by a light-blue cube. These 3d layers are stacked along the w direction (i.e., the extra spatial dimension) and coupled by interlayer *BF* terms (wavy lines), giving rise to two (3+1)D boundaries labeled as w_1 and w_2 . Panel (a) shows Toeplitz particle-loop braiding between a loop excitation (red) on the w_1 boundary and a particle excitation (red) on the w_2 boundary. A nontrivial braiding phase arises when the particle (red) is adiabatically transported such that its *induced boundary trajectory* (blue) on the *opposite* boundary—namely, the projected “shadow” of the particle (red) onto the w_1 boundary—winds around the loop (red). This process is encoded in the lower-left elements of K^{-1} , highlighted in panel (c). Panel (b) depicts the opposite configuration, encoded in the upper-right elements of K^{-1} highlighted in panel (d). Panel (e) summarizes the correspondence between the boundary localization of left and right zero singular modes (LZSMs and RZSMs), the structure of K^{-1} , and the resulting Toeplitz particle-loop braiding. These summarized results are higher-dimensional generalization of Toeplitz braiding introduced in Ref. [110].

in Fig. 1(a). When this induced boundary trajectory adiabatically winds around the loop excitation, a nontrivial braiding phase is accumulated. Crucially, the robustness of this phase depends only on the winding topology of the induced boundary trajectory and is independent of the separation between the particle and the loop along the w direction. From a field-theoretic perspective, in this work, we introduce the “infinite-component *BF* field theory” (iBF) to describe the above Toeplitz braiding.

The usual (3+1)D multi-component *BF* theories [126, 127] provide a versatile framework for describing 3d topological orders. Analogous to the (2+1)D Chern-Simons description of 2d systems, when pointlike and loop excitations are represented as charges and fluxes of an Abelian finite gauge group, the *BF* theory and its twisted variants [123, 128–137] form a unified field-theoretic scheme for capturing 3d topological orders and *gauged* SPT phases. A finite set of canonical *BF* terms BdA (with 2-form B and 1-form A fields), together with twisted terms such as $AA\bar{d}A$, AAA , AAB , BB , and the θ -term $d\bar{d}A$, encodes rich topological data—including particle-loop, multi-loop, and Borromean rings braiding [127, 130, 134, 138–151], emergent fermionic statistics [131, 136, 152, 153], and topological responses [123, 129, 137, 154–158]. Refs. [159–161] further showed how global symmetries fractionalize on loop excitations, introducing “mixed three-loop braiding”, which underlies the classification of higher-dimensional SET phases. These braiding processes obey stringent consistency conditions [135] ensuring gauge invariance and allowing for non-Abelian fusion and shrinking rules even when loop charges remain Abelian [134, 162]. Building on this foundation, a diagrammatic representation for higher-dimensional topological orders—including 4d cases [163]—was recently developed in Ref. [164].

To this end, we generalize the above established multi-component *BF* framework to an iBF theory—to describe 4d FTOs and Toeplitz braiding phenomena. In analogy to the iCS construction, we couple multi-component (3+1)D *BF* theories to formulate an effective field theory for 4d FTOs: $S = \int \frac{A_{I,J}}{2\pi} b^I \wedge da^J$. Stacking N layers of such (3+1)D field theories and coupling neighboring 3d “layers” via interlayer *BF* terms while preserving translational symmetry yields a multi-component *BF* theory characterized by a Toeplitz K matrix with integer elements:

$$S = \int \frac{K_{I,J}}{2\pi} b^I \wedge da^J, K = \begin{pmatrix} A & C & & & \\ B & A & C & & \\ & B & A & C & \\ & & \ddots & \ddots & \ddots \\ & & & B & A & C \\ & & & & B & A \end{pmatrix}. \quad (2)$$

Here N denotes the number of layers, also referred to as the “system size”. Taking $N \rightarrow \infty$ defines the *infinite-component BF theory*, i.e., iBF theory. The stacking process is illustrated in Figs. 1(a) and (b), where OBC is imposed along the w direction. Each blue cube represents

a 3d “layer” of BF theory on a three-torus where periodic boundary condition (PBC) is applied along x , y , and z , and the wavy lines denote interlayer BF couplings. A detailed discussion of particle–loop braiding and the construction of iBF theory is given in Sec. II.

Given an iBF theory with nearest-neighbor coupling, a natural question arises: *under what conditions does nonlocal braiding along the stacking direction emerge? Is there an analogue of boundary-mode-induced nonlocal braiding—i.e., Toeplitz braiding—along the stacking direction?* To address this, we classify iBF theories into two types. The first involves symmetric K matrices, where $C = B^T$ in Eq. (2); in this case, the Toeplitz braiding analysis parallels that of iCS theories [110], except that the particle–particle braiding of Ref. [110] now corresponds to particle–loop braiding in the BF context.

As shown in Sec. III, when K becomes asymmetric—sharing the same mathematical structure as the one-dimensional Hatano–Nelson (HN) [165] or non-Hermitian Su–Schrieffer–Heeger (nSSH)² [166, 167] Hamiltonians—the singular value decomposition (SVD) [168] of K reveals *boundary zero singular modes* (ZSMs)³ that give rise to nonlocal braiding along the stacking (w) direction. This phenomenon, also termed *Toeplitz braiding*, cannot be captured by boundary zero eigenmodes, emphasizing the necessity of the SVD perspective.

When all “left” ZSMs (LZSMs) localize on one w boundary and “right” ZSMs (RZSMs) on the other⁴, either the lower-left or upper-right elements of K^{-1} decay exponentially with system size. Consequently, nontrivial braiding arises when particles and loops occupy specific opposite w boundaries, as illustrated in Figs. 1(a)–1(b). The corresponding braiding phases are encoded in the lower-left or upper-right elements of K^{-1} [Figs. 1(c)–1(d)]. In either case, exchanging the particle and loop positions rapidly suppresses the braiding phase upon increasing the size of the w direction. In particular, iBF theories with K matrices resembling the nSSH Hamiltonians can exhibit nontrivial Toeplitz braiding in both configurations shown schematically in Figs. 1(a) and 1(b), as the K matrices may host two LZSMs (RZSMs) that localize at distinct w boundaries. The relation between the locations of the LZSMs and RZSMs, the patterns of K^{-1} , and the resulting braiding statistics is summarized in Fig. 1(e).

Interestingly, the same mathematical structure also appears in non-Hermitian directional amplification in driven–dissipative systems [169–172]. When ZSMs arise in such non-Hermitian Hamiltonians, driven–dissipative cavity arrays may exhibit directional amplification of

coherent inputs, with the gain growing exponentially with system size, whereas reversing the input direction markedly suppresses the effect.

The paper is organized as follows. Sec. II establishes the braiding structure of multi-component BF theories and introduces the stacking construction that gives rise to iBF field theories, emphasizing why non-diagonal Toeplitz K matrices are essential. Sec. III and Sec. IV uncover Toeplitz braiding in iBF theories whose K matrices inherit the mathematical structures of the HN and nSSH Hamiltonians, respectively. These sections show how SVD sharply exposes boundary zero singular modes and reveal a direct analogy to non-Hermitian directional amplification. Sec. V closes with a brief summary and outlook.

II. BRAIDING IN iBF THEORIES

A. Multi-component BF theories

In 3d Abelian topological orders, the topological excitations include both particles and loops; the BF theory naturally captures the associated Aharonov–Bohm particle–loop braiding phase. The partition function of a multi-component BF theory⁵ is

$$Z = \int \mathcal{D}b^I \mathcal{D}a^J e^{iS_{BF}}, \quad S_{BF} = \int \frac{K_{I,J}}{2\pi} b^I \wedge da^J. \quad (3)$$

Here K is a general $N \times N$ matrix (not necessarily Toeplitz), whose constraints will be determined below. Repeated indices I, J are implicitly summed over. The fields b^I and a^J ($I, J = 1, \dots, N$) are compact $U(1)$ 2-form and 1-form gauge fields obeying the Dirac quantization conditions

$$\oint db^I \in 2\pi\mathbb{Z}, \quad \oint da^I \in 2\pi\mathbb{Z}. \quad (4)$$

Their gauge transformations are $b^I \rightarrow b^I + d\beta^I$ and $a^I \rightarrow a^I + d\alpha^I$, where β^I (1-form) and α^I (0-form) are compact gauge parameters obeying $\oint d\beta^I \in 2\pi\mathbb{Z}$ and $\oint d\alpha^I \in 2\pi\mathbb{Z}$. Under these transformations, the action changes only by a boundary term: $S_{BF} \rightarrow S_{BF} + \frac{K_{I,J}}{2\pi} \int d\beta^I \wedge da^J$. Placing the theory on $S^2 \times S^2$ and decomposing the integral along the two spheres immediately requires $K_{I,J} \in \mathbb{Z}$, ensuring gauge invariance of the partition function.

The observables are Wilson operators

$$W(\gamma, \omega) = \exp \left[i \int_{\omega} L_I b^I + i \int_{\gamma} N_I a^I \right]$$

² In this paper, SSH only stands for *Hermitian* Su–Schrieffer–Heeger.

³ By ZSMs, we always mean modes from boundaries to avoid lengthy abbreviation such as BZSM.

⁴ Here the “left” and the “right” label internal sectors of the SVD rather than spatial sides.

⁵ While a single-component BF theory usually suffices for a given 3+1D spacetime, the multi-component generalization is essential for our construction of Toeplitz braiding. A related example is the charge–loop excitation symmetry in Ref. [123].

$$= \exp \left[i \int L_I b^I \wedge \delta\omega + i \int N_I a^I \wedge \delta\gamma \right], \quad (5)$$

where γ is a closed 1d loop and ω a closed 2d surface. The delta forms $\delta\omega$ and $\delta\gamma$ are supported only on these manifolds. Gauge invariance of $W(\gamma, \omega)$ requires $L_I, N_I \in \mathbb{Z}$. A topological excitation is thus either a particle labeled by $\mathbf{N} = (N_1, \dots, N_N)^\top$ or a closed loop labeled by $\mathbf{L} = (L_1, \dots, L_N)^\top$, whose worldline and worldsheet are γ and ω , respectively. The expectation value reads

$$\langle W(\gamma, \omega) \rangle = \frac{1}{Z} \int \mathcal{D}b^I \mathcal{D}a^J W(\gamma, \omega) e^{iS_{BF}}. \quad (6)$$

where Z is the partition function for the purpose of normalization. Integrating out b^I gives $L_I \delta\omega + \frac{K_{I,J}}{2\pi} da^J = 0$, so that $da^I = -2\pi(K^{-1})_{I,J} L_J \delta\omega$. Under a proper gauge choice, the solution is $a^I = -2\pi(K^{-1})_{I,J} L_J \delta\Omega$, where Ω is a Seifert hypersurface bounded by ω ($\partial\Omega = \omega$). Hence,

$$\langle W(\gamma, \omega) \rangle = \exp \left[-2\pi i N_I (K^{-1})_{I,J} L_J \int \delta\Omega \wedge \delta\gamma \right]. \quad (7)$$

The integral $\int \delta\Omega \wedge \delta\gamma$ equals the linking number between Ω and γ . Thus, the Aharonov–Bohm phase between a particle and a loop is [123]

$$2\pi N_I (K^{-1})_{I,J} L_J = 2\pi \mathbf{N}^\top K^{-1} \mathbf{L}. \quad (8)$$

This shows that particle–loop braiding phases are encoded in K^{-1} , directly analogous to particle–particle braiding in (2+1)D multi-component Chern–Simons theories.

B. Construction of infinite-component BF theories

As outlined in Sec. I, the iBF theory arises from coupling multi-component (3+1)D BF theories of the form $S = \int \frac{A_{I,J}}{2\pi} b^I \wedge da^J$, where b^I and a^J denote compact $U(1)$ 2-form and 1-form gauge fields, respectively. Here A is a square integer matrix, and repeated indices I, J are summed over. By stacking N layers of 3d topological orders described by these BF theories and introducing interlayer BF couplings that preserve translational symmetry along the stacking direction, we obtain a multi-component BF theory characterized by an integer Toeplitz K matrix that encodes the braiding statistics of topological excitations, as given in Eq. (2).

Taking the number of layers $N \rightarrow \infty$ defines the *infinite-component BF theory* (iBF theory). In the upcoming discussions, taking the thermodynamic limit refers specifically to sending N to infinity, as each individual layer is already in its own thermodynamic limit. The analysis in Sec. III follows this framework: first compute K^{-1} for finite N , then study the $N \rightarrow \infty$ limit to extract asymptotic braiding behavior. In what follows, we denote the stacking direction as the w axis and label

the two boundaries as the w_1 and w_2 boundaries. A loop or particle excitation $(1, 0, \dots, 0)^\top$ is assigned to the w_1 boundary, while $(0, 0, \dots, 1)^\top$ lies on the w_2 boundary. As a result, the indices of the components of the charge vectors \mathbf{N} and \mathbf{L} carry the meaning of w coordinates.

Fig. 1 schematically illustrates this stacking and particle–loop braiding process: each layer is a 3-torus (blue cubes in Figs. 1(a)–(b)), the wavy lines represent interlayer BF terms, and the stacking direction is the w axis. Here, we introduce a useful quantity, $\Theta_{I,J}$, which encodes the spatial distribution of particle–loop braiding phases along the w direction:

$$\Theta_{I,J} = 2\pi(K^{-1})_{I,J}. \quad (9)$$

With proper 2π shift, $\Theta_{I,J}$ is defined in $(-\pi, \pi]$ unless otherwise specified. More precisely, $\Theta_{I,J}$ is the braiding phase between a particle carrying unit charge located at w coordinate I and a loop carrying unit charge located at w coordinate J . The particle and loop vectors are given respectively:

$$\mathbf{N} = (0, 0, \dots, 1, \dots, 0, 0)^\top, \quad (10a)$$

$$\mathbf{L} = (0, 0, \dots, 1, \dots, 0, 0)^\top. \quad (10b)$$

where the two entries 1’s are respectively located at the I^{th} and J^{th} components of \mathbf{N} and \mathbf{L} i.e., $N_{I'} = \delta_{I,I'}, L_{J'} = \delta_{J,J'}$. Accordingly, the braiding between a loop at the w_1 boundary and a particle at the w_2 boundary [Fig. 1(a)] is encoded in the lower-left elements of K^{-1} as well as the matrix Θ [Fig. 1(c)], while the reverse configuration [Fig. 1(b)] corresponds to the upper-right elements [Fig. 1(d)].

Before analyzing specific iBF theories, we emphasize the necessity of considering non-diagonal Toeplitz K matrices in Eq. (2). Conventional multi-component BF theories possess a “relabeling redundancy” [123]: if two different K matrices denoted as K and K' of the same size $N \times N$, are related by two independent $GL(N, \mathbb{Z})$ transformations Ω, W ($|\det \Omega| = |\det W| = 1, W_{I,J}, \Omega_{I,J} \in \mathbb{Z}$) as $K' = \Omega K W^\top$, and the particle and loop charge vectors transform as $\mathbf{N}' = W \mathbf{N}$ and $\mathbf{L}' = \Omega \mathbf{L}$. Then we obtain identical braiding phases, $2\pi \mathbf{N}'^\top K'^{-1} \mathbf{L}' = 2\pi \mathbf{N}^\top K^{-1} \mathbf{L}$. Since any integer matrix can be brought to its Smith normal form via $GL(N, \mathbb{Z})$ transformations, one can normally decouple mutual BF terms by such diagonalization and study the diagonalized K matrix. However, by noting that I, J indices now label the w coordinates for iBF theories, preserving locality along the stacking direction restricts the allowed $GL(N, \mathbb{Z})$ transformations for Toeplitz K matrices [Eq. (2)]: Ω and W must be quasi-diagonal, with nonzero elements only clustered near the main diagonal.

To conclude this section, we point out the above diagonalization transformations on the Toeplitz matrix K via $GL(N, \mathbb{Z})$ cannot be found for the nontrivial Toeplitz braiding situation where K^{-1} possesses nonzero elements in either the upper-right or lower-left corners (see Fig. 1).

This conclusion can be straightforwardly proved via *reductio ad absurdum*: if a Toeplitz K is brought to its Smith normal form Λ (with nonzero elements only on the main diagonal) by quasi-diagonal Ω and W , i.e., $\Lambda = \Omega K W^\top$ or equivalently $K^{-1} = W^\top \Lambda^{-1} \Omega$. Obviously, due to the above-mentioned properties of W and Ω , K^{-1} has nonzero elements only clustered near the main diagonal. This, in turn, forbids any possible nonzero elements in the upper-right or lower-left corners, contradicting the existence of the nonzero upper-right and lower-left elements responsible for nontrivial Toeplitz braiding as shown in Fig. 1. Hence, non-diagonal Toeplitz K matrices are essential for the existence of the nontrivial Toeplitz braiding of iBF theories.

III. iBF THEORY WITH HATANO-NELSON TYPE K MATRIX

As described in Sec. I, we classify the K matrices of iBF theories into two types. The first type consists of symmetric K matrices, where $C = B^\top$ in Eq. (2). In this case, the analysis of Toeplitz braiding parallels that in iCS theories [110], except that the particle–particle braiding discussed in Ref. [110] is now reinterpreted as particle–loop braiding in the BF framework. When K is asymmetric, however, the particle–loop braiding phase is no longer invariant under exchanging the w coordinates of the particle and the loop, because K^{-1} is also asymmetric. As we will show, the presence of ZSMs leads to nonlocal braiding along the w direction. All detailed relations are summarized in Fig. 1.

In this section and following section, we demonstrate these features using two representative examples: the iBF theory with a HN-type K matrix and that with a nSSH-type K matrix. Both of them arise from coupling multi-component BF theories [Eq. (2)] with either $A = n$ or $A = \begin{pmatrix} A_{11} & A_{12} \\ A_{21} & A_{22} \end{pmatrix}$, $\det A \neq 0$. For a 2×2 integer matrix A of this form, its Smith normal form is $\begin{pmatrix} d_1 & 0 \\ 0 & d_2 \end{pmatrix}$, where $d_1 = \gcd(A_{11}, A_{12}, A_{21}, A_{22})$ and $d_2 = |A_{11}A_{22} - A_{12}A_{21}|/\gcd(A_{11}, A_{12}, A_{21}, A_{22})$ [173]. Hence, the corresponding BF theory effectively describes a $d_1 \times d_2$ gauge theory.

A. Toeplitz braiding and ZSMs—a concrete example

We use a concrete example—iBF constructed by coupling \mathbb{Z}_n topological orders—to demonstrate the correspondence between ZSMs and nonlocal braiding statistics in stacking direction. Before taking the $N \rightarrow \infty$ limit,

the K matrix of the iBF theory writes

$$K_{\text{HN}} = \begin{pmatrix} n & & & & \\ b & n & & & \\ & b & n & & \\ & & \ddots & \ddots & \\ & & & b & n \\ & & & & b & n \end{pmatrix}. \quad (11)$$

It is worth noting that the K matrix in Eq. (11) shares the same mathematical form with the Hamiltonian of Hatano-Nelson model [165]

$$K'_{\text{HN}} = \begin{pmatrix} n & c & & & & \\ b & n & c & & & \\ & b & n & c & & \\ & & \ddots & \ddots & \ddots & \\ & & & b & n & c \\ & & & & b & n \end{pmatrix} \quad (12)$$

when $c = 0$. The inverse of K_{HN} encodes the particle-loop braiding statistics, which reads

$$(K_{\text{HN}}^{-1})_{I,J} = \begin{cases} \frac{1}{n} \left(-\frac{b}{n}\right)^{I-J}, & I \geq J; \\ 0, & I < J. \end{cases} \quad (13)$$

If $|b| > |n|$ together with $n \text{rad}(n) \nmid b^6$, a nontrivial braiding statistical phase between the particle and the loop arises. From the equation for braiding phase (Eq. (8)) together with the expression for K_{HN}^{-1} , only when a particle is placed on w_2 boundary and a loop is placed on w_1 boundary, the nontrivial braiding phase manifests. For example, the mutual braiding phase between a particle $\mathbf{N} = (0, \dots, 0, 1)^\top$ and a loop $\mathbf{L} = (1, 0, \dots, 0)^\top$ is $2\pi \frac{1}{n} \left(-\frac{b}{n}\right)^{N-1}$. In contrast, if the positions of the particle and the loop are exchanged, the nontrivial braiding statistical phase between them vanishes. For illustrative purpose, we depict the $\Theta_{I,J}$ matrix (defined in Eq. (9)) for K_{HN} specified by $n = 2, b = 3$ with system size $N = 80$ in Fig. 2(a), clearly demonstrating this nonlocal braiding feature in the w direction.

To deepen our understanding of the origin of this nonlocal braiding statistics, we dig into the SVD of K_{HN} matrix. The SVD of K_{HN} is written as $K_{\text{HN}} = \sum_{i=1}^N \sigma_i \mathbf{u}_i \mathbf{v}_i^\top = \sigma_1 \mathbf{u}_1 \mathbf{v}_1^\top + \sigma_2 \mathbf{u}_2 \mathbf{v}_2^\top + \dots$, where the left singular modes $\{\mathbf{u}_i\}$ and the right singular modes $\{\mathbf{v}_i\}$ are mutually orthogonal, i.e., $\mathbf{u}_i^\top \mathbf{u}_j = \delta_{i,j}$, $\mathbf{v}_i^\top \mathbf{v}_j = \delta_{i,j}$, and $\{\sigma_i\}$ are the corresponding singular values.

If $|b| > |n|$, K_{HN} possesses the following left singular mode \mathbf{u}_1 located at the w_1 boundary and right singular

⁶ Here $\text{rad}(n)$ denotes the product of the distinct prime factors of n . The condition $n \text{rad}(n) \nmid b$ simply means that b is not divisible by $n \text{rad}(n)$, such that the braiding phase angle $\Theta_{I,J}$ defined in Eq. (9) is not trivially equal to $0 \bmod 2\pi$.

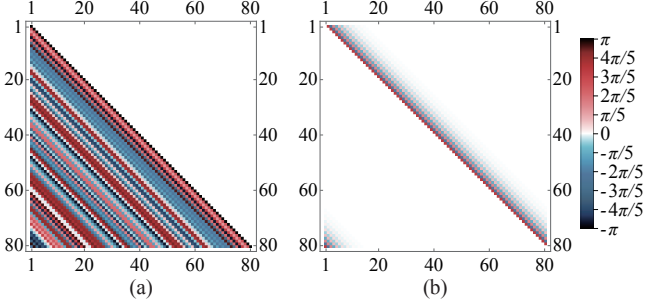


FIG. 2. Braiding phase $\Theta_{I,J} = 2\pi(K_{\text{HN}}^{-1})_{I,J}$ (Panel (a)) and $\Theta_{I,J} = 2\pi(K_{\text{HN,PBC}}^{-1})_{I,J}$ (Panel (b)) encoded in K_{HN} and $K_{\text{HN,PBC}}$ specified by $n = 2, b = 3$, where we select the system size $N = 80$ for illustrative purpose. The lower-left nonzero elements in Panel (b) corresponds to the braiding phases $\Theta_{I,J}$ between test particles and loops with w coordinates $I \sim N, J \sim 1$, which are close in the w direction due to PBC.

mode \mathbf{v}_1 located at the w_2 boundary when N is sufficiently large:

$$\mathbf{u}_1 = \sqrt{\frac{1 - (\frac{n}{b})^2}{1 - (\frac{n}{b})^{2N}}} \left(1 \ - \frac{n}{b} \ \cdots \ (-\frac{n}{b})^{N-1} \right)^T, \quad (14)$$

$$\mathbf{v}_1 = \sqrt{\frac{1 - (\frac{n}{b})^2}{1 - (\frac{n}{b})^{2N}}} \left((-\frac{n}{b})^{N-1} \ (-\frac{n}{b})^{N-2} \ \cdots \ 1 \right)^T. \quad (15)$$

Detailed calculation is presented in Appendix A 1. Moreover, the corresponding singular value σ_1 is obtained from

$$\sigma_1 = \mathbf{u}_1^T K_{\text{HN}} \mathbf{v}_1 = \frac{1 - (\frac{n}{b})^2}{1 - (\frac{n}{b})^{2N}} n \left(\frac{-n}{b} \right)^{N-1}. \quad (16)$$

The singular modes such as \mathbf{u}_1 and \mathbf{v}_1 that reside at the boundaries, decay exponentially into the bulk, and have singular values approaching zero in the thermodynamic limit $N \rightarrow \infty$ are referred to as ZSMs, as introduced in Sec. 1B. Left and right ZSMs are abbreviated LZSM and RZSM, respectively⁷. For large N , we can construct an approximate matrix M_{HN} from σ_1, \mathbf{u}_1 and \mathbf{v}_1 to model the large-size behavior of K^{-1} :

$$M_{\text{HN}} = \frac{1}{\sigma_1} \mathbf{v}_1 \mathbf{u}_1^T, \quad (M_{\text{HN}})_{I,J} = \frac{1}{n} \left(-\frac{b}{n} \right)^{I-J}. \quad (17)$$

M_{HN} represents the ZSM contribution to the inverse $K_{\text{HN}}^{-1} = \sum_{i=1}^N \sigma_i^{-1} \mathbf{v}_i \mathbf{u}_i^T = \sigma_1^{-1} \mathbf{v}_1 \mathbf{u}_1^T + \sigma_2^{-1} \mathbf{v}_2 \mathbf{u}_2^T + \cdots$. We observe that $(M_{\text{HN}})_{I,J} = (K_{\text{HN}}^{-1})_{I,J}$ for $I \geq J$, which

implies the braiding statistics between particles placed on the w_2 boundary and loops placed on the w_1 boundary are indeed encoded in ZSMs and the corresponding exponentially small singular value.

Furthermore, to emphasize the crucial role of ZSMs in generating nonlocal braiding statistics, we impose PBC along the w direction and isolate the bulk contribution to the inverse of K_{HN} . Under PBC, the Hatano-Nelson-type K matrix becomes

$$K_{\text{HN,PBC}} = \begin{pmatrix} n & & & & & b \\ b & n & & & & \\ & b & n & & & \\ & & \ddots & \ddots & & \\ & & & b & n & \\ & & & & b & n \end{pmatrix}, \quad (18)$$

and the w boundaries together with ZSMs are absent. In the large N limit, the inverse of $K_{\text{HN,OBC}}$ is

$$(K_{\text{HN,PBC}}^{-1})_{I,J} = \begin{cases} -\frac{1}{n} \left(-\frac{n}{b} \right)^{N-(I-J)}, & I \geq J; \\ -\frac{1}{n} \left(-\frac{n}{b} \right)^{J-I}, & I < J. \end{cases} \quad (19)$$

The formula for $(K_{\text{HN,PBC}}^{-1})_{I,J}$ indicates the mutual braiding phases $\Theta_{I,J}$ between test particles and loops which are well-separated along the w direction become negligibly small. As an illustration, Fig. 2(b) displays $\Theta_{I,J}$ for $K_{\text{HN,PBC}}$ with parameters $n = 2, b = 3$, and system size $N = 80$. Thus, braiding statistics is effectively local in the w direction when ZSMs are absent, underscoring the necessity of ZSMs in nonlocal braiding statistics along w .

B. General theory of Toeplitz braiding and ZSMs

Given a more general example, how can we understand the correspondence between ZSMs and nonlocal braiding statistics along the stacking direction in a more general framework? For more general iBF theories with Toeplitz K matrices, the connection between nonlocal braiding statistics and ZSMs can also be understood from the SVD of the K matrix. The SVD of an arbitrary $N \times N$ matrix K (not necessarily Toeplitz) is written as $K = \sum_{i=1}^N \sigma_i \mathbf{u}_i \mathbf{v}_i^T = \sigma_1 \mathbf{u}_1 \mathbf{v}_1^T + \sigma_2 \mathbf{u}_2 \mathbf{v}_2^T + \cdots$, where the left singular modes $\{\mathbf{u}_i\}$, right singular modes $\{\mathbf{v}_i\}$ and the corresponding singular values $\{\sigma_i\}$ of K are determined by [171, 174] $K \mathbf{v}_i = \sigma_i \mathbf{u}_i, K^T \mathbf{u}_i = \sigma_i \mathbf{v}_i, i = 1, \dots, N$. All singular modes can be chosen to be mutually orthogonal, i.e., $\mathbf{u}_i^T \mathbf{u}_j = \delta_{i,j}, \mathbf{v}_i^T \mathbf{v}_j = \delta_{i,j}$. The singular values are nonnegative by definition, and for any real matrix the corresponding singular modes can be chosen to be real⁸.

⁷ The “left” and “right” here refer to internal SVD sectors as is introduced in Sec. 1B, and are not related to the spatial distribution of the ZSMs (see Footnote 3). The LZSMs, RZSMs and the singular values discussed in this work may differ from the conventional definitions by a sign, which can be migrated among them without affecting the corresponding terms in SVD.

⁸ As the K matrices in this work are real matrices, we use the transpose (T) rather than the Hermitian conjugate (\dagger) in all expressions related to the SVD of Toeplitz K matrices hereafter.

Moreover, the LZSMs, RZSMs and the singular values in this paper may differ from the conventional definitions by a sign, which can be migrated among them without affecting the corresponding terms in SVD.

In the following, LZSMs are denoted by $\mathbf{u}_1, \mathbf{u}_2, \dots$ and the RZSMs are denoted by $\mathbf{v}_1, \mathbf{v}_2, \dots$. For finite system size N , we write $K = \sum_i \sigma_i \mathbf{u}_i \mathbf{v}_i^\top$, so its inverse is given by $K^{-1} = \sum_i \sigma_i^{-1} \mathbf{v}_i \mathbf{u}_i^\top$. If the K matrix possesses ZSMs, and all the LZSMs and RZSMs, namely \mathbf{u}_j and \mathbf{v}_j , are located at the opposite w boundaries, the ZSMs and their exponentially small singular values dominate the contribution to upper-right or lower-left elements of K^{-1} .

More specifically, if all the LZSMs localize at w_1 boundary and all the RZSMs localize at w_2 boundary, then, the ZSMs and their exponentially small singular values dominate the contribution to lower-left elements of K^{-1} (see Fig. 1(e) **column 1**); if all the LZSMs localize at w_2 boundary and all the RZSMs localize at w_1 boundary, then, the ZSMs and their exponentially small singular values dominate the contribution to upper-right elements of K^{-1} (see Fig. 1(e) **column 2**). In both cases, the bulk modes contribute exponentially small values to lower-left or upper-right elements of K^{-1} . That is,

$$(K^{-1})_{I,J} \approx \left(\sum_{j \in \text{ZSMs}} \frac{1}{\sigma_j} \mathbf{v}_j \mathbf{u}_j^\top \right)_{I,J} \quad (20)$$

for $I \sim 1, J \sim Nd$ or $I \sim Nd, J \sim 1$, where d is the size of the block A , block B and block C in Eq. (2). Therefore, the corresponding particle-loop braiding phase $\Theta_{I,J} = 2\pi(K^{-1})_{I,J}$, is also dominated by the contribution of ZSMs.

In particular, certain K matrices can support multiple LZSMs localized at both w boundaries, with RZSMs exhibiting similar pattern (see Fig. 1(e) **column 3**). In this case, nonzero elements exist for both the upper-right and lower-left regions of K^{-1} . These elements, together with the corresponding particle-loop braiding phases, are also dominated by the contributions from ZSMs. Concrete examples of this case are presented in Sec. IV.

It is noteworthy that the presence of ZSMs does not necessarily lead to nontrivial braiding statistics between particles and loops located at opposite w boundaries, since ZSMs alone do not guarantee the existence of noninteger elements in the upper-right or lower-left elements of K^{-1} , which are required for nontrivial braiding statistics. If the upper-right and lower-left elements of K^{-1} are all integers, the corresponding braiding phases $2\pi(K^{-1})_{I,J}$ trivially take values of multiples of 2π , which indicates that the nontrivial particle-loop braiding phases vanish for particles and loops placed sufficiently far away in the w direction. For example, if $n \text{ rad}(n) \mid b$, the $(K_{\text{HN}}^{-1})_{I,J}$ in Eq. (13) is integer for sufficiently large $|I - J|$. More concretely, K_{HN} with $n = 2, b = 4$ is an example where ZSMs are present but nonlocal braiding statistics along w direction is absent. The braiding phase $\Theta_{I,J} = \pi \delta_{I,J}$ is

nonzero only for $I = J$, indicating that nontrivial braiding statistics is nontrivial only for particles and loops residing in the same layer. Nevertheless, such special cases are very dilute in the whole parameter space; hence, the appearance of ZSMs indeed indicates nonlocal braiding statistics along the w direction in most cases.

The same mathematical structure emerges in non-Hermitian directional amplification studies, which stem from researches in driven-dissipative systems [169–172]. 1D driven-dissipative cavity arrays can display directional amplification of coherent inputs, with gains detected at the other boundary scale exponentially with system size. When the input is switched to the other end, the amplification effect is suppressed. Moreover, such exotic amplification effect absent in Hermitian systems can also be naturally understood from the singular value decomposition of the non-Hermitian Hamiltonian H . In systems with non-Hermitian directional amplification, the SVD spectrum of H under OBC exhibits ZSMs, whose corresponding LZSMs $\{\mathbf{u}_j\}$ and RZSMs $\{\mathbf{v}_j\}$, localize exponentially at opposite edges. In the linear-response regime, the susceptibility $\chi = H^{-1} = \sum_j \sigma_j^{-1} \mathbf{v}_j \mathbf{u}_j^\top$ is thus dominated by contributions from these ZSMs, leading to exponentially large, unidirectional transmission between boundaries [171]. This SVD-based framework provides a mathematically transparent diagnosis to directional amplification of physical signals in driven-dissipative systems.

C. Numerical results

In Fig. 3, we demonstrate the Toeplitz braiding encoded in iBF theories with K matrices sharing the same mathematical form of more general Hatano-Nelson Hamiltonians (Eq. (12)), verifying the results obtained from analytic deduction.

Panels (a1)–(e1) demonstrate the braiding statistics encoded in HN-type iBF theories with the K'_{HN} matrix specified by $n = 5, b = 1, c = 5$. (a1) and (b1) are the plots of the singular modes of the corresponding K'_{HN} matrix, and ZSMs are highlighted in red. (c1) is the matrix plot of the braiding phase $\Theta_{I,J} = 2\pi(K'_{\text{HN}})^{-1}_{I,J}$ introduced in Eq. (9). The presence of nontrivial braiding phases in the upper-right region of K'_{HN}^{-1} indicates that there exist particle excitations located at w_1 boundary and loop excitations located at w_2 boundary, which can feel each other via braiding process. In contrast, the absence of the upper-right components of K'_{HN}^{-1} shows that the braiding phase vanishes when particle's and loop's w coordinates are exchanged. As the $\#$ of layers N goes to infinity, the braiding phase $\Theta_{1,N}$ in (d1) oscillates between $(-\pi, \pi]$, while $\Theta_{N,1}$ in (e1) rapidly decays to zero.

Likewise, Panels (a2)–(e2) demonstrate the braiding statistics encoded in NH-type iBF theories with the K'_{HN} matrix specified by $n = 5, b = 5, c = 1$, in which particle excitations located at w_2 boundary and loop excita-

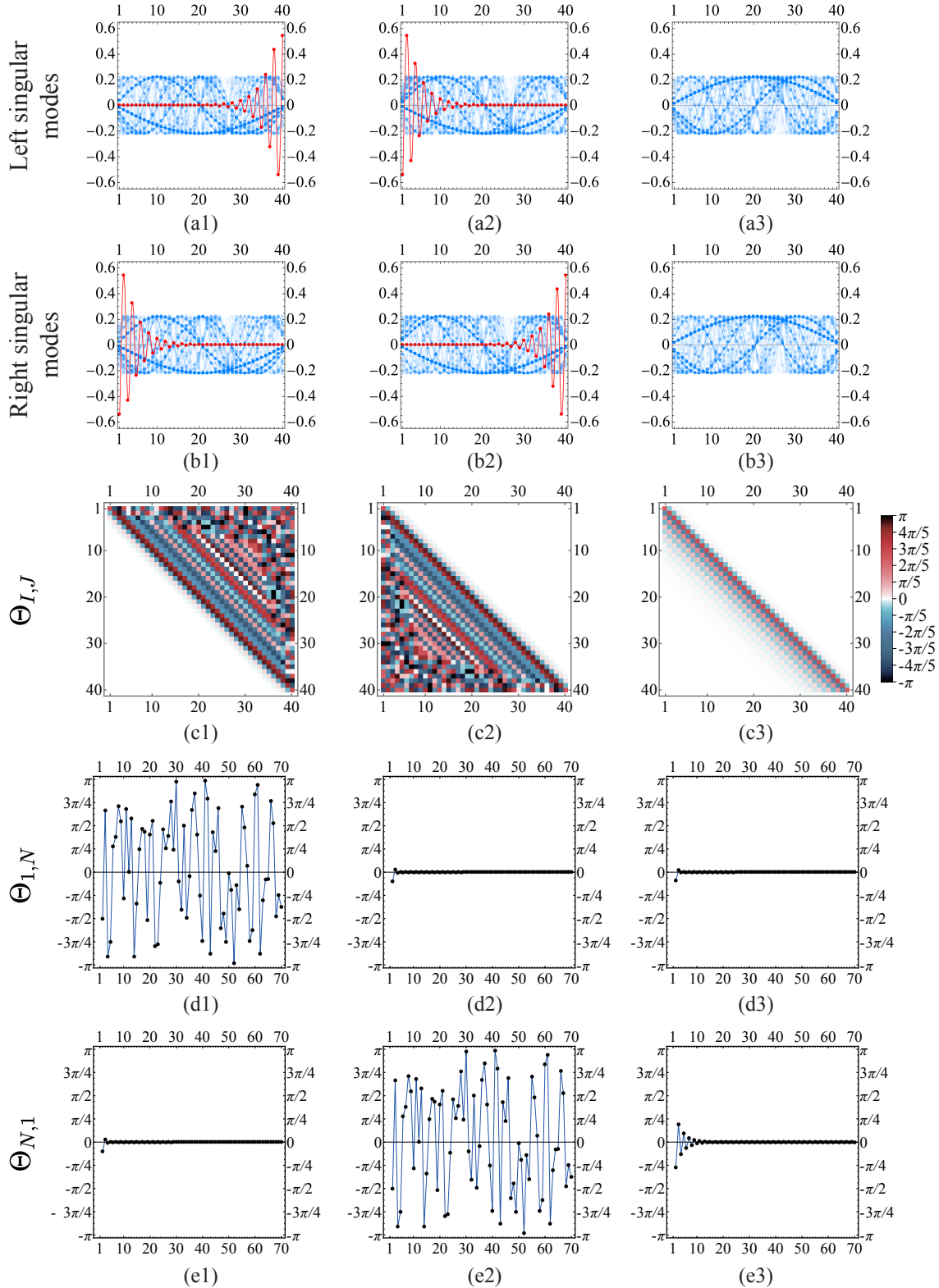


FIG. 3. Braiding statistics encoded in iBF theories with Hatano-Nelson-type (HN-type) K matrices. (a1)–(e1) and (a2)–(e2) demonstrate the Toeplitz braiding encoded in HN-type iBF theories, with the K'_{HN} matrix specified by the parameters $n = 5$, $b = 1$, $c = 5$ and $n = 5$, $b = 5$, $c = 1$, respectively. (a3)–(e3) demonstrates a trivial iBF theory with K'_{HN} matrix specified by $n = 5$, $b = 3$ and $c = 1$. (a1)–(a3) are the plots of the left singular modes of these matrices, while (b1)–(b3) are the plots of the right singular modes of these matrices. (c1)–(c3) are the matrix plots of the braiding phases $\Theta_{I,J} = 2\pi(K'_{\text{HN}})^{-1}_{I,J}$. For illustrative purpose, we take the system size N to be 40. (d1)–(d3) and (e1)–(e3) demonstrate how the braiding phases $\Theta_{1,N}$ and $\Theta_{N,1}$ vary as the system size N increases.

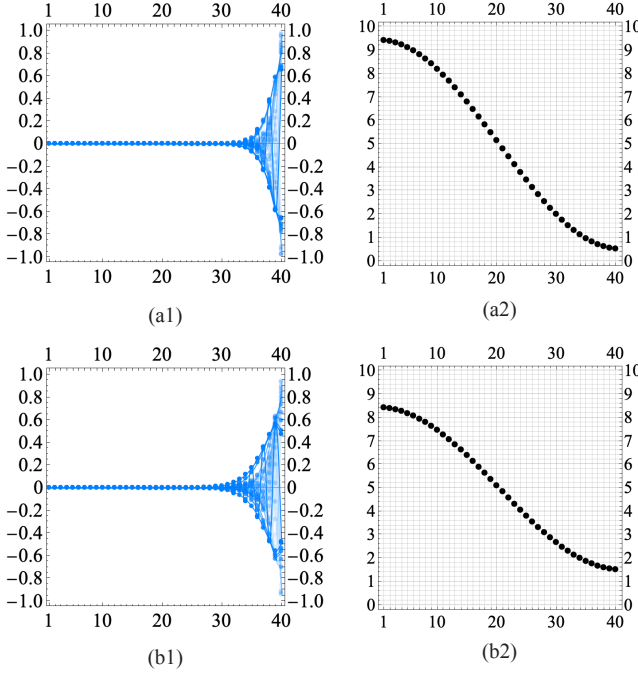


FIG. 4. (a1) and (a2) display skin modes and eigenvalues of K'_{HN} matrix specified by $n = 5, b = 5, c = 1$. (b1) and (b2) display skin modes and eigenvalues of K'_{HN} matrix specified by $n = 5, b = 3, c = 1$. For illustrative purpose, we depict the skin modes and eigenvalues of the K'_{HN} matrices with system size $N = 40$.

tions located at w_1 boundary that can feel each other via braiding process. (a2) and (b2) are the plots of the singular modes of the K'_{HN} matrix, and ZSMs are highlighted in red. (c2) is the matrix plot of the braiding phase $\Theta_{I,J} = 2\pi(K'_{\text{HN}}^{-1})_{I,J}$ introduced in Eq. (9). The presence of nontrivial braiding phases in the lower-left region of K'_{HN}^{-1} indicates that there exist particle excitations located at w_2 boundary and loop excitations located at w_1 boundary, which can feel each other via braiding process. In contrast, the absence of the upper-right components of K'_{HN}^{-1} shows that the braiding phase vanishes when particle's and loop's w coordinates are exchanged. As the # of layers N goes to infinity, the braiding phase $\Theta_{N,1}$ in (e2) oscillates between $(-\pi, \pi]$, while $\Theta_{1,N}$ in (d2) rapidly decays to zero.

For comparison, we also present an iBF theory without Toeplitz braiding in Panels (a3)–(e3). The corresponding K'_{HN} matrix is obtained by the parameters $n = 5, b = 3$, and $c = 1$. Panels (a3) and (b3) display the singular modes of the K'_{HN} matrix, where ZSMs are absent. The exponentially suppressed upper-right and lower-left elements in Panel (c3) indicate the absence of nonlocal braiding statistics along the stacking direction, which is further reflected in the asymptotic convergence of $\Theta_{1,N}$ and $\Theta_{N,1}$, as shown in Panels (d3) and (e3).

To furthermore highlight the importance and necessity of SVD in analyzing Toeplitz braiding encoded in asym-

metric K matrices, the skin modes and eigenvalues of the K'_{HN} matrices are shown in Fig. 4. Figures 4(a1) and 4(a2) display the skin modes [175–186] and eigenvalues of the K'_{HN} matrix with parameters $n = 5, b = 5$, and $c = 1$, whose corresponding braiding statistics is illustrated in Figs. 3(a2)–(e2). Similarly, Figs. 4(b1) and 4(b2) show the skin modes and eigenvalues of the K'_{HN} matrix with parameters $n = 5, b = 3$, and $c = 1$, whose braiding statistics is illustrated in Figs. 3(a3)–(e3). As seen from these comparisons, the skin modes and eigenvalues of the K matrices of iBF theories with and without Toeplitz braiding exhibit qualitatively similar features. Therefore, adopting the singular value decomposition perspective of the K matrices is essential for a complete characterization.

IV. IBF THEORY WITH NON-HERMITIAN SU-SCHRIEFFER-HEEGER TYPE K MATRIX

A. Toeplitz Braiding encoded in Su-Schrieffer-Heeger type K matrix

To gain further insight into Toeplitz braiding encoded in asymmetric K matrices, we now turn to another analytically tractable example, which has richer phase structure as the parameters in K change. The K matrix of such iBF theory is

$$K_{\text{nSSH}} = \begin{pmatrix} A & C & & & \\ B & A & C & & \\ & B & A & C & \\ & & \ddots & \ddots & \ddots \\ & & & B & A & C \\ & & & & B & A \end{pmatrix}, \quad (21)$$

where the blocks A , B and C read

$$A = \begin{pmatrix} 0 & n_1 \\ n_2 & 0 \end{pmatrix}, \quad B = \begin{pmatrix} 0 & m_1 \\ 0 & 0 \end{pmatrix}, \quad C = \begin{pmatrix} 0 & 0 \\ m_2 & 0 \end{pmatrix}. \quad (22)$$

The K_{nSSH} matrix exhibits the same mathematical structure as that of the non-Hermitian SSH (nSSH) model [166, 167]. By applying Cramer's rule, one readily unveils the inverse of K_{nSSH} :

$$(K_{\text{nSSH}}^{-1})_{I,J} = \begin{cases} \frac{1}{n_1} \left(-\frac{m_1}{n_1} \right)^{\frac{I-J-1}{2}}, & I > J, I \in 2\mathbb{Z}^+, J \in 2\mathbb{Z}^+ - 1; \\ \frac{1}{n_2} \left(-\frac{m_2}{n_2} \right)^{\frac{J-I-1}{2}}, & I < J, I \in 2\mathbb{Z}^+ - 1, J \in 2\mathbb{Z}^+; \\ 0, & \text{others.} \end{cases} \quad (23)$$

For instance, when the system size $N = 4$, K_{nSSH}^{-1} reads

$$\begin{pmatrix} 0 & \frac{1}{n_2} & 0 & -\frac{m_2}{n_2^2} & 0 & \frac{m_2^2}{n_2^3} & 0 & -\frac{m_2^3}{n_2^4} \\ \frac{1}{n_1} & 0 & 0 & 0 & 0 & 0 & 0 & 0 \\ 0 & 0 & 0 & \frac{1}{n_2} & 0 & -\frac{m_2}{n_2^2} & 0 & \frac{m_2^2}{n_2^3} \\ -\frac{m_1}{n_1^2} & 0 & \frac{1}{n_1} & 0 & 0 & 0 & 0 & 0 \\ 0 & 0 & 0 & 0 & 0 & \frac{1}{n_2} & 0 & -\frac{m_2}{n_2^2} \\ \frac{m_1^2}{n_1^3} & 0 & -\frac{m_1}{n_1^2} & 0 & \frac{1}{n_1} & 0 & 0 & 0 \\ 0 & 0 & 0 & 0 & 0 & 0 & 0 & \frac{1}{n_2} \\ -\frac{m_1^3}{n_1^4} & 0 & \frac{m_1^2}{n_1^3} & 0 & -\frac{m_1}{n_1^2} & 0 & \frac{1}{n_1} & 0 \end{pmatrix}. \quad (24)$$

The classification of K_{nSSH}^{-1} can be described across four parameter regimes, each determined by the relative magnitudes of $|m_1|$ and $|n_1|$ as well as $|m_2|$ and $|n_2|$. These parameter regimes, combined with the divisibility conditions described below, determine the presence or absence of Toeplitz braiding along the stacking direction.

Case I corresponds to $|m_1| > |n_1|$ and $|m_2| < |n_2|$, where the upper-right elements of K_{nSSH}^{-1} are suppressed and the lower-left elements increase exponentially with system size. In this regime, nontrivial braiding statistics occurs between particles at the w_2 boundary and loops at the w_1 boundary when $n_1 \text{ rad}(n_1) \nmid m_1$; otherwise, when $n_1 \text{ rad}(n_1) | m_1$, the braiding statistics between particles and loops at distinct w boundaries is trivial.

Case II arises when $|m_1| < |n_1|$ and $|m_2| > |n_2|$, leading to K_{nSSH}^{-1} with exponentially suppressed lower-left elements, while the upper-right elements increase exponentially with the system size. Here, particles at the w_1 boundary can braid nontrivially with loops at the w_2 boundary if $n_2 \text{ rad}(n_2) \nmid m_2$, while exchanging the w coordinates of the particles and the loops yields trivial statistics. If $n_2 \text{ rad}(n_2) | m_2$, the braiding statistics between particles and loops at distinct w boundaries is trivial.

Case III occurs when $|m_1| > |n_1|$ and $|m_2| > |n_2|$, so both nonzero upper-right and lower-left elements exist. In this regime, several possibilities arise: nontrivial braiding between w_2 -boundary particles and w_1 -boundary loops when $n_1 \text{ rad}(n_1) \nmid m_1$ but $n_2 \text{ rad}(n_2) | m_2$; nontrivial braiding between w_1 -boundary particles and w_2 -boundary loops when the conditions are reversed, i.e. $n_2 \text{ rad}(n_2) \nmid m_2$ but $n_1 \text{ rad}(n_1) | m_1$; nontrivial braiding statistics for both configurations of particles and loops located at distinct w boundaries when neither divisibility condition holds; fully trivial statistics between particles and loops at distinct w boundaries when both divisibility conditions hold.

Finally, **Case IV**, defined by $|m_1| < |n_1|$ and $|m_2| < |n_2|$, has both upper-right and lower-left elements of K_{nSSH}^{-1} suppressed and yields only trivial braiding statistics between particles and loops located at distinct w boundaries.

B. ZSMs and Toeplitz braiding

To deepen our understanding of the origin of this nonlocal braiding statistics along the w direction, i.e. Toeplitz braiding, the relation between ZSMs of the K matrices and Toeplitz braiding in iBF theories with nSSH-type K matrix is further investigated. In Appendix A 2, the ZSMs are derived analytically. In Case I where $\begin{cases} |m_1| > |n_1| \\ |m_2| < |n_2| \end{cases}$, K_{nSSH} possesses the following LZSM and RZSM, denoted by \mathbf{u}_1 and \mathbf{v}_1 , respectively.

$$\mathbf{u}_1 = \sqrt{\frac{1 - \frac{n_1^2}{m_1^2}}{1 - (\frac{n_1}{m_1})^{2N}}} \begin{pmatrix} 1 & 0 & -\frac{n_1}{m_1} & 0 & \cdots & \left(-\frac{n_1}{m_1}\right)^{N-1} & 0 \end{pmatrix}^T, \quad (25)$$

$$\mathbf{v}_1 = \sqrt{\frac{1 - \frac{m_2^2}{n_2^2}}{1 - (\frac{m_2}{n_2})^{2N}}} \begin{pmatrix} 0 & 1 & 0 & -\frac{m_2}{n_2} & \cdots & 0 & \left(-\frac{m_2}{n_2}\right)^{N-1} \end{pmatrix}^T. \quad (26)$$

In Case II where $\begin{cases} |m_1| < |n_1| \\ |m_2| > |n_2| \end{cases}$, K_{nSSH} possesses the following LZSM and RZSM, denoted by \mathbf{u}_2 and \mathbf{v}_2 , respectively.

$$\mathbf{u}_2 = \sqrt{\frac{1 - \frac{m_2^2}{n_2^2}}{1 - (\frac{m_2}{n_2})^{2N}}} \begin{pmatrix} 0 & 1 & 0 & -\frac{m_2}{n_2} & \cdots & 0 & \left(-\frac{m_2}{n_2}\right)^{N-1} \end{pmatrix}^T, \quad (27)$$

$$\mathbf{v}_2 = \sqrt{\frac{1 - \frac{n_2^2}{m_2^2}}{1 - (\frac{n_2}{m_2})^{2N}}} \begin{pmatrix} 1 & 0 & -\frac{n_2}{m_2} & 0 & \cdots & \left(-\frac{n_2}{m_2}\right)^{N-1} & 0 \end{pmatrix}^T. \quad (28)$$

In Case III where $\begin{cases} |m_1| > |n_1| \\ |m_2| > |n_2| \end{cases}$, the K_{nSSH} matrix possesses two sets of ZSMs, \mathbf{u}_1 , \mathbf{v}_1 and \mathbf{u}_2 , \mathbf{v}_2 . In Case IV where $\begin{cases} |m_1| < |n_1| \\ |m_2| < |n_2| \end{cases}$, the K_{nSSH} matrix possesses no ZSM. Furthermore, there is an exponentially small violation from the decaying tails of ZSMs to the opposite boundary, leading to exponentially small singular values σ_1 and σ_2 , which are obtained from

$$\sigma_1 = \mathbf{u}_1^T K_{\text{nSSH}} \mathbf{v}_1 = \sqrt{\frac{1 - \frac{m_1^2}{n_1^2}}{1 - (\frac{m_1}{n_1})^{2N}}} \sqrt{\frac{1 - \frac{n_1^2}{m_1^2}}{1 - (\frac{n_1}{m_1})^{2N}}} n_1, \quad (29)$$

$$\sigma_2 = \mathbf{u}_2^T K_{\text{nSSH}} \mathbf{v}_2 = \sqrt{\frac{1 - \frac{m_2^2}{n_2^2}}{1 - (\frac{m_2}{n_2})^{2N}}} \sqrt{\frac{1 - \frac{n_2^2}{m_2^2}}{1 - (\frac{n_2}{m_2})^{2N}}} n_2. \quad (30)$$

In line with Eq. (20), we construct an approximate matrix M_{nSSH} for the inverse K_{nSSH}^{-1} that captures the contribution of ZSMs to the upper-right or lower-left elements of

K_{nSSH}^{-1} . For Case I with $\begin{cases} |m_1| > |n_1| \\ |m_2| < |n_2| \end{cases}$, M_{nSSH} is constructed by \mathbf{u}_1 , \mathbf{v}_1 and σ_1 .

$$M_{\text{nSSH}} = \frac{1}{\sigma_1} \mathbf{v}_1 \mathbf{u}_1^\top, \quad (M_{\text{nSSH}})_{I,J} = \begin{cases} \frac{1}{n_1} \left(-\frac{m_1}{n_1} \right)^{(I-J-1)/2}, & I > J, I \in 2\mathbb{Z}^+, J \in 2\mathbb{Z}^+ - 1; \\ -\frac{1}{m_1} \left(-\frac{n_1}{m_1} \right)^{(J-I-1)/2}, & J > I, I \in 2\mathbb{Z}^+, J \in 2\mathbb{Z}^+ - 1; \\ 0, & \text{others.} \end{cases} \quad (31)$$

For example, if the system size $N = 4$,

$$M_{\text{nSSH}} = \begin{pmatrix} 0 & 0 & 0 & 0 & 0 & 0 & 0 & 0 \\ \frac{1}{n_1} & 0 & -\frac{1}{m_1} & 0 & \frac{n_1}{m_1^2} & 0 & -\frac{n_1^2}{m_1^3} & 0 \\ 0 & 0 & 0 & 0 & 0 & 0 & 0 & 0 \\ -\frac{m_1}{n_1^2} & 0 & \frac{1}{n_1} & 0 & -\frac{1}{m_1} & 0 & \frac{n_1}{m_1^2} & 0 \\ 0 & 0 & 0 & 0 & 0 & 0 & 0 & 0 \\ \frac{m_1^2}{n_1^3} & 0 & -\frac{m_1}{n_1^2} & 0 & \frac{1}{n_1} & 0 & -\frac{1}{m_1} & 0 \\ 0 & 0 & 0 & 0 & 0 & 0 & 0 & 0 \\ -\frac{m_1^3}{n_1^4} & 0 & \frac{m_2^2}{n_1^3} & 0 & -\frac{m_1}{n_1^2} & 0 & \frac{1}{n_1} & 0 \end{pmatrix}. \quad (32)$$

For Case II with $\begin{cases} |m_1| < |n_1| \\ |m_2| > |n_2| \end{cases}$, the approximate matrix M_{nSSH} is constructed by \mathbf{u}_2 , \mathbf{v}_2 and σ_2 .

$$M_{\text{nSSH}} = \frac{1}{\sigma_2} \mathbf{v}_2 \mathbf{u}_2^\top, \quad (M_{\text{nSSH}})_{I,J} = \begin{cases} \frac{1}{n_2} \left(-\frac{m_2}{n_2} \right)^{(J-I-1)/2}, & J > I, I \in 2\mathbb{Z}^+ - 1, J \in 2\mathbb{Z}^+; \\ -\frac{1}{m_2} \left(-\frac{n_2}{m_2} \right)^{(I-J-1)/2}, & I > J, I \in 2\mathbb{Z}^+ - 1, J \in 2\mathbb{Z}^+; \\ 0, & \text{others.} \end{cases} \quad (33)$$

For example, if system size $N = 4$,

$$M_{\text{nSSH}} = \begin{pmatrix} 0 & \frac{1}{n_2} & 0 & -\frac{m_2}{n_2^2} & 0 & \frac{m_2^2}{n_2^3} & 0 & -\frac{m_2^3}{n_2^4} \\ 0 & 0 & 0 & 0 & 0 & 0 & 0 & 0 \\ 0 & -\frac{1}{m_2} & 0 & \frac{1}{n_2} & 0 & -\frac{m_2}{n_2^2} & 0 & \frac{m_2^2}{n_2^3} \\ 0 & 0 & 0 & 0 & 0 & 0 & 0 & 0 \\ 0 & \frac{n_2}{m_2^2} & 0 & -\frac{1}{m_2} & 0 & \frac{1}{n_2} & 0 & -\frac{m_2}{n_2^2} \\ 0 & 0 & 0 & 0 & 0 & 0 & 0 & 0 \\ 0 & -\frac{n_2^2}{m_2^3} & 0 & \frac{n_2}{m_2^2} & 0 & -\frac{1}{m_2} & 0 & \frac{1}{n_2} \\ 0 & 0 & 0 & 0 & 0 & 0 & 0 & 0 \end{pmatrix}. \quad (34)$$

For Case III with $\begin{cases} |m_1| > |n_1| \\ |m_2| > |n_2| \end{cases}$, the approximate matrix M_{nSSH} is constructed by all \mathbf{u}_i , \mathbf{v}_i and σ_i ($i = 1, 2$).

$$M_{\text{nSSH}} = \frac{1}{\sigma_1} \mathbf{v}_1 \mathbf{u}_1^\top + \frac{1}{\sigma_2} \mathbf{v}_2 \mathbf{u}_2^\top, \quad (M_{\text{nSSH}})_{I,J} =$$

$$\begin{cases} \frac{1}{n_1} \left(-\frac{m_1}{n_1} \right)^{(I-J-1)/2}, & I > J, I \in 2\mathbb{Z}^+, J \in 2\mathbb{Z}^+ - 1; \\ -\frac{1}{m_1} \left(-\frac{n_1}{m_1} \right)^{(J-I-1)/2}, & J > I, I \in 2\mathbb{Z}^+, J \in 2\mathbb{Z}^+ - 1; \\ \frac{1}{n_2} \left(-\frac{m_2}{n_2} \right)^{(J-I-1)/2}, & J > I, I \in 2\mathbb{Z}^+ - 1, J \in 2\mathbb{Z}^+; \\ -\frac{1}{m_2} \left(-\frac{n_2}{m_2} \right)^{(I-J-1)/2}, & I > J, I \in 2\mathbb{Z}^+ - 1, J \in 2\mathbb{Z}^+; \\ 0, & \text{others.} \end{cases} \quad (35)$$

For example, if system size $N = 4$,

$$M_{\text{nSSH}} = \begin{pmatrix} 0 & \frac{1}{n_2} & 0 & -\frac{m_2}{n_2^2} & 0 & \frac{m_2^2}{n_2^3} & 0 & -\frac{m_2^3}{n_2^4} \\ \frac{1}{n_1} & 0 & -\frac{1}{m_1} & 0 & \frac{n_1}{m_1^2} & 0 & -\frac{n_1^2}{m_1^3} & 0 \\ 0 & -\frac{1}{m_2} & 0 & \frac{1}{n_2} & 0 & -\frac{m_2}{n_2^2} & 0 & \frac{m_2^2}{n_2^3} \\ -\frac{m_1}{n_1^2} & 0 & \frac{1}{n_1} & 0 & -\frac{1}{m_1} & 0 & \frac{n_1}{m_1^2} & 0 \\ 0 & \frac{n_2}{m_2^2} & 0 & -\frac{1}{m_2} & 0 & \frac{1}{n_2} & 0 & -\frac{m_2}{n_2^2} \\ \frac{m_1^2}{n_1^3} & 0 & -\frac{m_1}{n_1^2} & 0 & \frac{1}{n_1} & 0 & -\frac{1}{m_1} & 0 \\ 0 & -\frac{n_2^2}{m_2^3} & 0 & \frac{n_2}{m_2^2} & 0 & -\frac{1}{m_2} & 0 & \frac{1}{n_2} \\ -\frac{m_1^3}{n_1^4} & 0 & \frac{m_1^2}{n_1^3} & 0 & -\frac{m_1}{n_1^2} & 0 & \frac{1}{n_1} & 0 \end{pmatrix}. \quad (36)$$

For all the cases with Toeplitz braiding, in the thermodynamic limit $N \rightarrow \infty$, M_{nSSH} approximates the lower-left elements of K_{nSSH}^{-1} up to exponentially suppressed terms when $|m_1| > |n_1|$, and approximates the upper-right elements of K_{nSSH}^{-1} up to exponentially suppressed terms when $|m_2| > |n_2|$. Therefore, ZSMs together with the corresponding exponentially small singular values, capture the braiding statistics between particles and loops residing at distinct w boundaries. In particular, Case III demonstrates that nontrivial Toeplitz braiding between particles and loops located at both w boundaries are possible, provided that two sets of ZSMs exist, and that both w boundaries host localized LZSMs (RZSMs).

It should be noticed that the presence of ZSMs is not a sufficient condition for nontrivial Toeplitz braiding. For instance, even the parameters in K_{nSSH} fall in Case I, as long as $n_1 \text{ rad}(n_1)|m_1|$, the lower-left elements of K_{nSSH}^{-1} are all integers, forbidding nontrivial Toeplitz braiding along the w direction. Nevertheless, such special cases are very dilute in the whole parameter space; hence, the appearance of ZSMs indeed indicates nonlocal braiding statistics along the w direction in most cases.

C. Numerical results

In Fig. 5, we depict several examples that demonstrate the nonlocal braiding statistics induced by ZSMs, verifying the analytic deductions presented above. Panels (a1)–(e1) demonstrates the braiding statistics encoded in nSSH-type iBF theories with the K_{nSSH} matrix specified by $n_1 = n_2 = 2$, $m_1 = 3$, $m_2 = 1$, which belongs

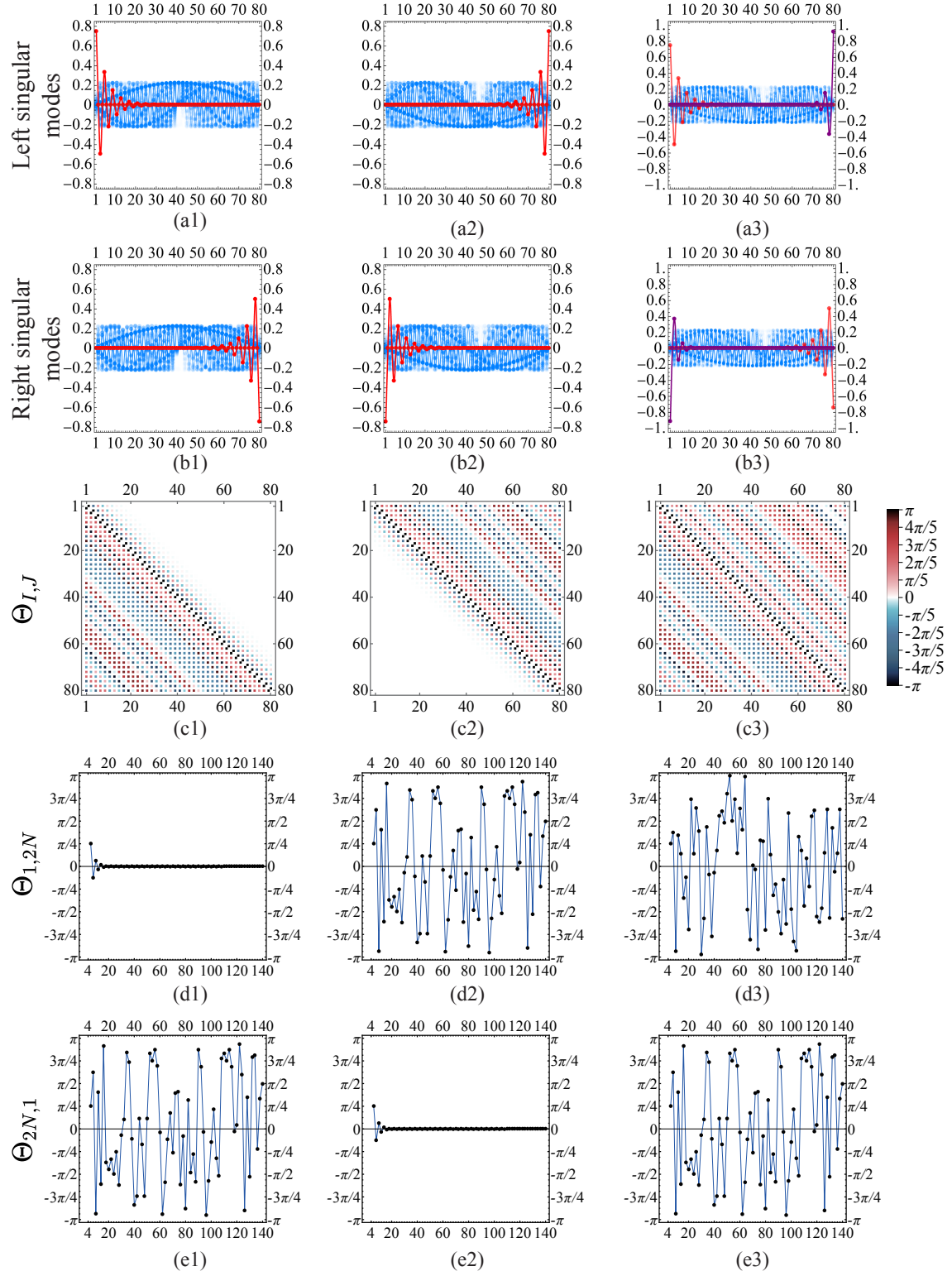


FIG. 5. Braiding statistics in different nSSH-type iBF theories. (a1)–(e1), (a2)–(e2) and (a3)–(e3) demonstrate the braiding statistics encoded in nSSH-type iBF theories with the K_{nSSH} matrix specified by $\begin{cases} n_1 = n_2 = 2 \\ m_1 = 3, m_2 = 5 \end{cases}$, respectively. (a1)–(a3) are the plots of the left singular modes of these matrices, while (b1)–(b3) are the plots of the right singular modes of these matrices. The ZSMs are highlighted in red and purple. (c1)–(c3) are the matrix plots of the braiding phase $\Theta_{I,J} = 2\pi(K_{\text{nSSH}}^{-1})_{I,J}$, where we take the system size $N = 40$ (the resulting matrix size of K_{nSSH} is $2N = 80$) as illustrative examples. (d1)–(d3) and (e1)–(e3) demonstrate how the braiding phases $\Theta_{1,2N}$ and $\Theta_{2N,1}$ vary as the system size N increases.

to Case I. (a1) and (b1) are the plots of the singular modes of the K_{nSSH} matrix, where ZSMs are highlighted in red. (c1) is the matrix plot of the braiding phase $\Theta_{I,J} = 2\pi(K_{\text{nSSH}}^{-1})_{I,J}$ (Eq. (9)). The presence of nontrivial braiding phases in the lower-left region of $\Theta_{I,J}$ indicates that there exist particle excitations located at w_2 boundary and loop excitations located at w_1 boundary that can feel each other via braiding process. In contrast, the absence of a nontrivial braiding phase in the upper-right region of $\Theta_{I,J}$ shows that when their w coordinates are exchanged, the braiding phase vanishes. (d1) shows that as the size $2N$ of the matrix increases, the braiding phase $\Theta_{1,2N}$ drastically decays to zero as the system size increases, while (e1) shows that the braiding phase $\Theta_{2N,1}$ oscillates between $(-\pi, \pi]$, reflecting the non-liquid nature of the *iBF* theory.

Likewise, Panels (a2)–(e2) demonstrates the braiding statistics encoded in nSSH-type *iBF* theories with the K_{nSSH} matrix specified by $n_1 = n_2 = 2, m_1 = 1, m_2 = 3$, which belongs to Case II. (a2) and (b2) are the plots of the singular modes of such K_{nSSH} matrix, where ZSMs are highlighted in red. (c2) is the matrix plot of the braiding phase $\Theta_{I,J} = 2\pi(K_{\text{nSSH}}^{-1})_{I,J}$. The presence of nontrivial braiding phases in the upper-right region of $\Theta_{I,J}$ indicates that there exist particle excitations located at w_1 boundary and loop excitations located at w_2 boundary that can feel each other via braiding process. In contrast, the absence of a nontrivial braiding phase in the lower-left region of $\Theta_{I,J}$ shows that when their w coordinates are exchanged, the braiding phase vanishes. (d2) shows that as the system size N increases, the braiding phase $\Theta_{1,2N}$ oscillates between $(-\pi, \pi]$, while (e2) shows that the braiding phase $\Theta_{2N,1}$ drastically decays to zero as the system size N increases.

Panels (a3)–(e3) demonstrates the braiding statistics encoded in nSSH-type *iBF* theories with the K_{nSSH} matrix specified by $n_1 = n_2 = 2, m_1 = 3, m_2 = 5$, which belongs to Case III. In this case, the K_{nSSH} matrix possesses two sets of ZSMs, highlighted in red and purple in Panels (a3) and (b3). Nontrivial braiding statistics arises for both configurations: particles at w_1 boundary with loops at w_2 boundary, and vice versa, as is demonstrated in the matrix plot (c3) of the braiding phase $\Theta_{I,J} = 2\pi(K_{\text{nSSH}}^{-1})_{I,J}$. (d3) and (e3) show that as the system size N increases, both $\Theta_{1,2N}$ and $\Theta_{2N,1}$ oscillate between $(-\pi, \pi]$.

D. Equivalence Between Eigendecomposition and SVD in Capturing Toeplitz Braiding for Symmetric K matrix

So far, we focus on the role of ZSMs in nonlocal braiding statistics along the stacking direction. Ref. [110] shows that boundary zero modes obtained from eigendecomposition capture the upper-right and lower-left elements of K^{-1} in the thermodynamic limit when the K matrix is symmetric. Are these two approaches compat-

ible with each other? Are there any differences between the approximate matrix M constructed from ZSMs and the approximate matrix M' constructed from boundary zero modes when the K matrix is symmetric? In fact, Eqs. (A2) and (A9) in Appendix A are equations for the boundary zero modes of the Hermitian K matrices, thus these two approaches are indeed identical. We explicitly verify this using K_{nSSH} for the case $n_1 = n_2 = n$ and $m_1 = m_2 = m$. When $n_1 = n_2 = n$ and $m_1 = m_2 = m$, K_{nSSH} (Eq. (21)) is a symmetric matrix sharing the same mathematical form of the SSH Hamiltonian [187]. If $|m| > |n|$, the approximate matrix M'_{nSSH} for the inverse K_{nSSH}^{-1} constructed from boundary zero modes \mathbf{w}_1 and \mathbf{w}_2 reads [110]

$$M'_{\text{nSSH}} = \frac{1}{\lambda_1} \mathbf{w}_1 \mathbf{w}_1^\top + \frac{1}{\lambda_2} \mathbf{w}_2 \mathbf{w}_2^\top, \quad (37)$$

where

$$\mathbf{w}_1 = \frac{1}{\sqrt{2}} \sqrt{\frac{1 - \left(\frac{n}{m}\right)^2}{1 - \left(\frac{n}{m}\right)^{2N}}} \left(1, \left(-\frac{n}{m}\right)^{N-1}, \left(-\frac{n}{m}\right), \left(-\frac{n}{m}\right)^{N-2}, \left(-\frac{n}{m}\right)^2, \dots, \left(-\frac{n}{m}\right)^{N-1}, 1\right)^\top, \quad (38a)$$

$$\mathbf{w}_2 = \frac{1}{\sqrt{2}} \sqrt{\frac{1 - \left(\frac{n}{m}\right)^2}{1 - \left(\frac{n}{m}\right)^{2N}}} \left(-1, \left(-\frac{n}{m}\right)^{N-1}, \frac{n}{m}, \left(-\frac{n}{m}\right)^{N-2}, \dots, \left(-\frac{n}{m}\right), -\left(-\frac{n}{m}\right)^{N-1}, 1\right)^\top. \quad (38b)$$

and the exponentially small eigenvalues are

$$\lambda_1 = n \frac{1 - \left(\frac{n}{m}\right)^2}{1 - \left(\frac{n}{m}\right)^{2N}} \left(-\frac{n}{m}\right)^{N-1}, \quad (39)$$

$$\lambda_2 = -n \frac{1 - \left(\frac{n}{m}\right)^2}{1 - \left(\frac{n}{m}\right)^{2N}} \left(-\frac{n}{m}\right)^{N-1}. \quad (40)$$

The approximate matrix constructed from ZSMs is given by Eq. (35). Comparing M_{nSSH} and M'_{nSSH} , we discover that

$$(M_{\text{nSSH}})_{I,J} = (M'_{\text{nSSH}})_{I,J} = \begin{cases} \frac{1}{n} \left(-\frac{m}{n}\right)^{(I-J-1)/2}, & I > J, I \in 2\mathbb{Z}^+, J \in 2\mathbb{Z}^+ - 1; \\ -\frac{1}{m} \left(-\frac{m}{n}\right)^{(I-J-1)/2}, & I > J, I \in 2\mathbb{Z}^+ - 1, J \in 2\mathbb{Z}^+; \\ \frac{1}{n} \left(-\frac{m}{n}\right)^{(J-I-1)/2}, & J > I, J \in 2\mathbb{Z}^+, I \in 2\mathbb{Z}^+ - 1; \\ -\frac{1}{m} \left(-\frac{m}{n}\right)^{(J-I-1)/2}, & J > I, J \in 2\mathbb{Z}^+ - 1, I \in 2\mathbb{Z}^+; \\ 0, & \text{others.} \end{cases} \quad (41)$$

For example, if the system size is $N = 4$, M_{nSSH} , M'_{nSSH} are of size $2N = 8$,

$$M'_{\text{nSSH}} = M_{\text{nSSH}} =$$

$$\begin{pmatrix} 0 & \frac{1}{n} & 0 & -\frac{m}{n^2} & 0 & \frac{m^2}{n^3} & 0 & -\frac{m^3}{n^4} \\ \frac{1}{n} & 0 & -\frac{1}{m} & 0 & \frac{n}{m^2} & 0 & -\frac{n^2}{m^3} & 0 \\ 0 & -\frac{1}{m} & 0 & \frac{1}{n} & 0 & -\frac{m}{n^2} & 0 & \frac{m^2}{n^3} \\ -\frac{m}{n^2} & 0 & \frac{1}{n} & 0 & -\frac{1}{m} & 0 & \frac{n}{m^2} & 0 \\ 0 & \frac{n}{m^2} & 0 & -\frac{1}{m} & 0 & \frac{1}{n} & 0 & -\frac{m}{n^2} \\ \frac{m^2}{n^3} & 0 & -\frac{m}{n^2} & 0 & \frac{1}{n} & 0 & -\frac{1}{m} & 0 \\ 0 & -\frac{n^2}{m^3} & 0 & \frac{n}{m^2} & 0 & -\frac{1}{m} & 0 & \frac{1}{n} \\ -\frac{m^3}{n^4} & 0 & \frac{m^2}{n^3} & 0 & -\frac{m}{n^2} & 0 & \frac{1}{n} & 0 \end{pmatrix}, \quad (42)$$

demonstrating that these two approaches are indeed identical if K_{SSH} is symmetric.

V. CONCLUSION AND OUTLOOK

In this paper, we investigated four-dimensional fracton topological orders within the framework of infinite-component BF (iBF) theories and identified boundary zero singular modes (ZSMs) as the fundamental mechanism underlying nonlocal braiding statistics along the stacking direction, which we term “Toeplitz braiding”. A defining feature of Toeplitz-braiding iBF theories is their extreme boundary sensitivity and directionality: nontrivial particle-loop braiding phases arise only when the excitations occupy specific opposite boundaries along the stacking direction, while exchanging their boundary locations causes the braiding phase to vanish in the thermodynamic limit. We demonstrated that, for asymmetric Toeplitz K matrices, the ZSM sector dominates the off-diagonal corner structure of K^{-1} at large system size, thereby encoding the essential braiding data of particles and loops residing on opposite boundaries. Through combined analytical and numerical studies of iBF theories with Hatano–Nelson and non-Hermitian Su–Schrieffer–Heeger-type K matrices, we established a sharp and universal correspondence between the existence and boundary localization of ZSMs and the emergence of nontrivial Toeplitz braiding phases. These results elevate stacking constructions of topological field theories from a descriptive tool to a predictive framework for engineering exotic braiding phenomena in higher dimensions. More broadly, identifying ZSMs as the operative degrees of freedom behind Toeplitz braiding provides a unifying principle that connects fracton physics and topological field theory with non-Hermitian physics, particularly directional amplification phenomena.

Beyond condensed-matter realizations, we propose an intriguing conjecture: iBF theories may be interpreted as describing a family of entangled parallel universes [188]. In this picture, intralayer loop excitations play the role of cosmic strings: they carry invisible charges and do not exert dynamical forces on particles, yet they generate nontrivial Aharonov–Bohm phases when enclosed by charged-particle trajectories [139]. In contrast, interlayer loop excitations carrying gauge charges can be viewed as wormholes [189] connecting adjacent universes,

as they represent topological defects that alter the connectivity along the stacking direction. The interlayer BF couplings then correspond to condensates of such wormholes, with the coupling strength controlling the effective tunneling amplitude between neighboring universes. This “wormhole condensation” picture is analogous to the anyon-condensation mechanism in multilayer fractional quantum Hall systems [112]. From this perspective, iBF theories with Toeplitz braiding describe parallel universes whose mutual tunneling is strong enough that cosmic strings in one universe can imprint robust topological phase factors on charged particles in another, even when the universes are far apart.

Several directions merit future exploration. A natural next step is to construct explicit lattice realizations of iBF theories that support Toeplitz braiding, enabling direct numerical studies and potentially guiding experimental implementations. Conversely, it is equally worthwhile to develop field-theoretical approaches, including iBF theory, to revisit topics extensively studied in lattice settings—such as generalized entanglement renormalization [16] and foliation structures [5, 102, 103]—in the context of four-dimensional fracton topological orders. In this work we focused on particle-loop braiding arising from stacking *pure* BF theories. Extending the construction by incorporating twisted terms to realize multi-loop and Borromean-rings braiding remains an open problem [130, 134, 135, 142, 153, 162–164, 190, 191]. Another intriguing direction is to incorporate global or subsystem symmetries into iBF theories and to explore the resulting symmetry-fractionalization patterns.

ACKNOWLEDGMENTS

P.Y. thanks Liujun Zou and Ching Hua Lee for insightful discussions during his visit to the National University of Singapore. This work was partially supported by the National Natural Science Foundation of China (NSFC) under Grant No. 12474149, the Research Center for Magnetoelectric Physics of Guangdong Province under Grant No. 2024B0303390001, and the Guangdong Provincial Key Laboratory of Magnetoelectric Physics and Devices under Grant No. 2022B1212010008.

Appendix A: Detailed calculation on ZSMs

1. Detailed calculation on ZSMs of HN-type K matrices

Left singular modes and right singular modes denoted by \mathbf{u} and \mathbf{v} are determined by $K_{\text{HN}}\mathbf{v} = \sigma\mathbf{u}$, $K_{\text{HN}}^{\top}\mathbf{u} = \sigma\mathbf{v}$, respectively. These equations render

$$K_{\text{HN}}K_{\text{HN}}^{\top}\mathbf{u} = \sigma^2\mathbf{u}, \quad K_{\text{HN}}^{\top}K_{\text{HN}}\mathbf{v} = \sigma^2\mathbf{v}. \quad (\text{A1})$$

Therefore, determining the singular modes \mathbf{u} and \mathbf{v} is equivalent to finding the eigenmodes of the Hermitian

matrices $K_{\text{HN}}K_{\text{HN}}^T$ and $K_{\text{HN}}^T K_{\text{HN}}$. One can then adopt the customary technique from the study of boundary zero modes of Hermitian systems. Since we focus on the ZSMs denoted by \mathbf{u}_1 and \mathbf{v}_1 with exponentially small singular values ($\det K_{\text{HN}} \neq 0$), the $\sigma \rightarrow 0$ is taken before further calculation. Furthermore, multiplying the equations in Eq. (A1) by K_{HN}^{-1} and $(K_{\text{HN}}^{-1})^T$, respectively, we obtain

$$K_{\text{HN}}^T \mathbf{u}_1 = 0, \quad K_{\text{HN}} \mathbf{v}_1 = 0. \quad (\text{A2})$$

Assume the solution of boundary zero mode takes the form

$$\mathbf{u}_1 = (u_1, u_2, \dots, u_N)^T, \quad \mathbf{v}_1 = (v_1, v_2, \dots, v_N)^T. \quad (\text{A3})$$

Eq. (A2) renders

$$\begin{cases} bu_j + nu_{j-1} = 0, & j = 2, 3, \dots, N; \\ nu_N = 0; \end{cases} \quad (\text{A4a})$$

$$\begin{cases} nv_1 = 0; \\ bv_{j-1} + nv_j = 0, & j = 2, 3, \dots, N. \end{cases} \quad (\text{A5a})$$

$$\begin{cases} nv_1 = 0; \\ bv_{j-1} + nv_j = 0, & j = 2, 3, \dots, N. \end{cases} \quad (\text{A5b})$$

Eq. (A4a) is solved by $u_j = (-\frac{n}{b})^{j-1}$ for $j = 1, \dots, N$. If $|b| > |n|$, Eq. (A4b) is only violated by exponentially small terms before taking thermodynamic limit $N \rightarrow \infty$. Because eigenspectra and eigenstates of Hermitian matrices are stable under small perturbations of matrix elements, one may slightly adjust the matrix elements to absorb this exponentially small violation. This operation does not severely alter the eigenspectrum or the eigenstates of the original matrix $K_{\text{HN}}K_{\text{HN}}^T$. In the thermodynamic limit $N \rightarrow \infty$, Eq. (A4b) is strictly satisfied. Therefore, in the case $|b| > |n|$, the following normalized solution to LZSM appears:

$$\mathbf{u}_1 = \sqrt{\frac{1 - (\frac{n}{b})^2}{1 - (\frac{n}{b})^{2N}}} \left(1 \ - \frac{n}{b} \ \dots \ (-\frac{n}{b})^{N-1} \right)^T. \quad (\text{A6})$$

Likewise, in the case $|b| > |n|$, the following normalized solution to RZSM appears:

$$\mathbf{v}_1 = \sqrt{\frac{1 - (\frac{n}{b})^2}{1 - (\frac{n}{b})^{2N}}} \left((-\frac{n}{b})^{N-1} \ (-\frac{n}{b})^{N-2} \ \dots \ 1 \right)^T. \quad (\text{A7})$$

Another point worth noting is that Eq. (A2) resembles those used to solve for boundary zero modes of Hermitian matrices. However, the zero modes obtained from Eq. (A2) are not necessarily the true zero eigenmodes of K_{HN}^T and K_{HN} , as the eigenspectra and eigenstates of non-Hermitian matrices are highly sensitive under even exponentially small perturbations of matrix elements. Therefore, the exponentially small violations may not be absorbed by a slight modification of the matrix elements of K_{HN}^T and K_{HN} .

2. Detailed calculation on ZSMs of nSSH-type K matrices

Left singular modes and right singular modes denoted by \mathbf{u} and \mathbf{v} are determined by $K_{\text{nSSH}}\mathbf{v} = \sigma\mathbf{u}$, $K_{\text{nSSH}}^T\mathbf{u} = \sigma\mathbf{v}$, respectively. These equations render

$$K_{\text{nSSH}}K_{\text{nSSH}}^T\mathbf{u} = \sigma^2\mathbf{u}, \quad K_{\text{nSSH}}^T K_{\text{nSSH}}\mathbf{v} = \sigma^2\mathbf{v}. \quad (\text{A8})$$

In the thermodynamic limit $N \rightarrow \infty$, the singular values of ZSMs approach zero, i.e. $\sigma \rightarrow 0$. Since we focus on the ZSMs denoted by \mathbf{u} and \mathbf{v} with exponentially small singular values ($\det K_{\text{nSSH}} \neq 0$), the $\sigma \rightarrow 0$ is taken before further calculation. For the same reason described in Appendix A 1, the above two equations yield

$$K_{\text{nSSH}}^T\mathbf{u} = 0, \quad K_{\text{nSSH}}\mathbf{v} = 0. \quad (\text{A9})$$

Denote the components of \mathbf{v} and \mathbf{u} as

$$\begin{aligned} \mathbf{u} &= (u_{1,A} \ u_{1,B} \ \dots \ u_{N,A} \ u_{N,B})^T, \\ \mathbf{v} &= (v_{1,A} \ v_{1,B} \ \dots \ v_{N,A} \ v_{N,B})^T. \end{aligned} \quad (\text{A10})$$

The bulk recurrence relation encoded in the equation $K_{\text{nSSH}}^T\mathbf{u} = 0$ is

$$\begin{aligned} & \begin{pmatrix} 0 & m_2 \\ 0 & 0 \end{pmatrix} \begin{pmatrix} u_{j-1,A} \\ u_{j-1,B} \end{pmatrix} + \begin{pmatrix} 0 & n_2 \\ n_1 & 0 \end{pmatrix} \begin{pmatrix} u_{j,A} \\ u_{j,B} \end{pmatrix} \\ & + \begin{pmatrix} 0 & 0 \\ m_1 & 0 \end{pmatrix} \begin{pmatrix} u_{j+1,A} \\ u_{j+1,B} \end{pmatrix} = 0, \quad j = 2, 3, \dots, N-1. \end{aligned} \quad (\text{A11})$$

The ansatz for $(u_{j,A} \ u_{j,B})^T$ is

$$(u_{j,A} \ u_{j,B})^T = \beta^j (u_A \ u_B)^T, \quad (\text{A12})$$

which renders

$$\begin{pmatrix} 0 & m_2\beta^{-1} + n_2 \\ n_1 + m_1\beta & 0 \end{pmatrix} \begin{pmatrix} u_A \\ u_B \end{pmatrix} = 0. \quad (\text{A13})$$

The condition for nontrivial solution is

$$\det \begin{pmatrix} 0 & m_2\beta^{-1} + n_2 \\ n_1 + m_1\beta & 0 \end{pmatrix} = 0, \quad (\text{A14})$$

and the solutions are

$$\beta_1 = -\frac{n_1}{m_1}, \quad \beta_2 = -\frac{m_2}{n_2}. \quad (\text{A15})$$

Hence the corresponding solution to u_A , u_B is

$$u_{A,1} = 1, \quad u_{B,1} = 0; \quad (\text{A16})$$

$$u_{A,2} = 0, \quad u_{B,2} = 1. \quad (\text{A17})$$

Denote the corresponding candidate boundary zero mode as \mathbf{u}_1 and \mathbf{u}_2 . If $|\beta_1| < 1$, $|m_1| > |n_1|$, the following

$$\mathbf{u}_1 = \sqrt{\frac{1 - \frac{n_1^2}{m_1^2}}{1 - (\frac{n_1}{m_1})^{2N}}} \left(1 \ 0 \ -\frac{n_1}{m_1} \ 0 \ \dots \ \left(-\frac{n_1}{m_1}\right)^{N-1} \ 0 \right)^T \quad (\text{A18})$$

is automatically a legitimate solution of LZSM, since the w_1 boundary equation is satisfied:

$$\begin{pmatrix} 0 & n_2 \\ n_1 & 0 \end{pmatrix} \begin{pmatrix} 1 \\ 0 \end{pmatrix} + \begin{pmatrix} 0 & 0 \\ m_1 & 0 \end{pmatrix} \begin{pmatrix} -\frac{n_1}{m_1} \\ 0 \end{pmatrix} = 0. \quad (\text{A19})$$

If $|\beta_2| > 1$, $|m_2| > |n_2|$, the following

$$\mathbf{u}_2 = \sqrt{\frac{1 - \frac{m_2^2}{n_2^2}}{1 - (\frac{m_2}{n_2})^{2N}}} \begin{pmatrix} 0 & 1 & 0 & -\frac{m_2}{n_2} & \cdots & 0 & \left(-\frac{m_2}{n_2}\right)^{N-1} \end{pmatrix}^\top \quad (\text{A20})$$

is automatically a legitimate solution to LZSM, since the w_2 boundary equation is satisfied:

$$\begin{aligned} & \begin{pmatrix} 0 & m_2 \\ 0 & 0 \end{pmatrix} \left(-\frac{m_2}{n_2}\right)^{N-1} \begin{pmatrix} 0 \\ 1 \end{pmatrix} \\ & + \begin{pmatrix} 0 & n_2 \\ n_1 & 0 \end{pmatrix} \left(-\frac{m_2}{n_2}\right)^N \begin{pmatrix} 0 \\ 1 \end{pmatrix} = 0. \end{aligned} \quad (\text{A21})$$

Hence there are at most two solutions to LZSM:

$$\mathbf{u}_1 = \sqrt{\frac{1 - \frac{n_1^2}{m_1^2}}{1 - (\frac{n_1}{m_1})^{2N}}} \begin{pmatrix} 1 & 0 & -\frac{n_1}{m_1} & 0 & \cdots & \left(-\frac{n_1}{m_1}\right)^{N-1} & 0 \end{pmatrix}^\top, \quad (\text{A22})$$

$$\mathbf{u}_2 = \sqrt{\frac{1 - \frac{m_2^2}{n_2^2}}{1 - (\frac{m_2}{n_2})^{2N}}} \begin{pmatrix} 0 & 1 & 0 & -\frac{m_2}{n_2} & \cdots & 0 & \left(-\frac{m_2}{n_2}\right)^{N-1} \end{pmatrix}^\top. \quad (\text{A23})$$

If $|m_1| > |n_1|$, the following \mathbf{u}_1 is a legitimate solution to LZSM. If $|m_2| > |n_2|$, the following \mathbf{u}_2 is automatically a legitimate solution to LZSM.

The discussion to $K_{\text{nSSH}}\mathbf{v} = 0$ is similar. The bulk recurrence relation encoded in the equation $K_{\text{nSSH}}\mathbf{v} = 0$ is

$$\begin{aligned} & \begin{pmatrix} 0 & m_1 \\ 0 & 0 \end{pmatrix} \begin{pmatrix} v_{j-1,A} \\ v_{j-1,B} \end{pmatrix} + \begin{pmatrix} 0 & n_1 \\ n_2 & 0 \end{pmatrix} \begin{pmatrix} v_{j,A} \\ v_{j,B} \end{pmatrix} \\ & + \begin{pmatrix} 0 & 0 \\ m_2 & 0 \end{pmatrix} \begin{pmatrix} v_{j+1,A} \\ v_{j+1,B} \end{pmatrix} = 0, \quad j = 2, 3, \dots, N-1. \end{aligned} \quad (\text{A24})$$

The ansatz for $(v_{j,A} \ v_{j,B})^\top$ is

$$(v_{j,A} \ v_{j,B})^\top = \beta^j (v_A \ v_B)^\top, \quad (\text{A25})$$

which renders

$$\begin{pmatrix} 0 & m_1\beta^{-1} + n_1 \\ n_2 + m_2\beta & 0 \end{pmatrix} \begin{pmatrix} v_A \\ v_B \end{pmatrix} = 0. \quad (\text{A26})$$

The condition for nontrivial solution is

$$\det \begin{pmatrix} 0 & m_1\beta^{-1} + n_1 \\ n_2 + m_2\beta & 0 \end{pmatrix} = 0, \quad (\text{A27})$$

and the solutions are

$$\beta_1 = -\frac{m_1}{n_1}, \quad \beta_2 = -\frac{n_2}{m_2}. \quad (\text{A28})$$

Hence the corresponding solution to v_A, v_B is

$$v_{A,1} = 0, \quad v_{B,1} = 1; \quad (\text{A29})$$

$$v_{A,2} = 1, \quad v_{B,2} = 0. \quad (\text{A30})$$

Denote the corresponding candidate boundary zero mode as \mathbf{v}_1 and \mathbf{v}_2 . If $|\beta_1| > 1$, $|m_1| > |n_1|$, the following \mathbf{v}_1

$$\mathbf{v}_1 = \sqrt{\frac{1 - \frac{m_1^2}{n_1^2}}{1 - (\frac{m_1}{n_1})^{2N}}} \begin{pmatrix} 0 & 1 & 0 & -\frac{m_1}{n_1} & \cdots & 0 & \left(-\frac{m_1}{n_1}\right)^{N-1} \end{pmatrix}^\top \quad (\text{A31})$$

is automatically a legitimate solution of RZSM, since the w_2 boundary equation

$$\begin{aligned} & \begin{pmatrix} 0 & m_1 \\ 0 & 0 \end{pmatrix} \left(-\frac{m_1}{n_1}\right)^{N-1} \begin{pmatrix} 0 \\ 1 \end{pmatrix} \\ & + \begin{pmatrix} 0 & n_1 \\ n_2 & 0 \end{pmatrix} \left(-\frac{m_1}{n_1}\right)^N \begin{pmatrix} 0 \\ 1 \end{pmatrix} = 0 \end{aligned} \quad (\text{A32})$$

is satisfied.

If $|\beta_2| < 1$, $|m_2| > |n_2|$, the following

$$\mathbf{v}_2 = \sqrt{\frac{1 - \frac{m_2^2}{n_2^2}}{1 - (\frac{m_2}{n_2})^{2N}}} \begin{pmatrix} 1 & 0 & -\frac{n_2}{m_2} & 0 & \cdots & \left(-\frac{n_2}{m_2}\right)^{N-1} & 0 \end{pmatrix}^\top \quad (\text{A33})$$

is automatically a legitimate solution to RZSM, since the w_1 boundary equation is automatically satisfied:

$$\begin{pmatrix} 0 & n_1 \\ n_2 & 0 \end{pmatrix} \begin{pmatrix} 1 \\ 0 \end{pmatrix} + \begin{pmatrix} 0 & 0 \\ m_2 & 0 \end{pmatrix} \begin{pmatrix} -\frac{n_2}{m_2} \\ 0 \end{pmatrix} = 0. \quad (\text{A34})$$

Hence there are at most two solutions to RZSMs:

$$\mathbf{v}_1 = \sqrt{\frac{1 - \frac{m_1^2}{n_1^2}}{1 - (\frac{m_1}{n_1})^{2N}}} \begin{pmatrix} 0 & 1 & 0 & -\frac{m_1}{n_1} & \cdots & 0 & \left(-\frac{m_1}{n_1}\right)^{N-1} \end{pmatrix}^\top, \quad (\text{A35})$$

$$\mathbf{v}_2 = \sqrt{\frac{1 - \frac{m_2^2}{n_2^2}}{1 - (\frac{m_2}{n_2})^{2N}}} \begin{pmatrix} 1 & 0 & -\frac{n_2}{m_2} & 0 & \cdots & \left(-\frac{n_2}{m_2}\right)^{N-1} & 0 \end{pmatrix}^\top. \quad (\text{A36})$$

In the case $|m_1| > |n_1|$, \mathbf{v}_1 is a legitimate RZSM. In the case $|m_2| > |n_2|$, \mathbf{v}_2 is a legitimate RZSM.

[1] R. M. Nandkishore and M. Hermele, Fractons, *Annual Review of Condensed Matter Physics* **10**, 295 (2019).

[2] C. Chamon, Quantum glassiness in strongly correlated clean systems: An example of topological overprotection, *Phys. Rev. Lett.* **94**, 040402 (2005).

[3] S. Vijay, J. Haah, and L. Fu, A new kind of topological quantum order: A dimensional hierarchy of quasiparticles built from stationary excitations, *Phys. Rev. B* **92**, 235136 (2015).

[4] S. Vijay, J. Haah, and L. Fu, Fracton topological order, generalized lattice gauge theory, and duality, *Phys. Rev. B* **94**, 235157 (2016).

[5] W. Shirley, K. Slagle, Z. Wang, and X. Chen, Fracton models on general three-dimensional manifolds, *Phys. Rev. X* **8**, 031051 (2018).

[6] H. Song, J. Schönmeier-Kromer, K. Liu, O. Viyuela, L. Pollet, and M. A. Martin-Delgado, Optimal thresholds for fracton codes and random spin models with subsystem symmetry, *Phys. Rev. Lett.* **129**, 230502 (2022).

[7] H. Ma, E. Lake, X. Chen, and M. Hermele, Fracton topological order via coupled layers, *Phys. Rev. B* **95**, 245126 (2017).

[8] W. Shirley, K. Slagle, and X. Chen, Foliated fracton order from gauging subsystem symmetries, *SciPost Phys.* **6**, 041 (2019).

[9] A. Prem, J. Haah, and R. Nandkishore, Glassy quantum dynamics in translation invariant fracton models, *Phys. Rev. B* **95**, 155133 (2017).

[10] A. Dua, I. H. Kim, M. Cheng, and D. J. Williamson, Sorting topological stabilizer models in three dimensions, *Phys. Rev. B* **100**, 155137 (2019).

[11] D. Bulmash and M. Barkeshli, Gauging fractons: Immobile non-abelian quasiparticles, fractals, and position-dependent degeneracies, *Phys. Rev. B* **100**, 155146 (2019).

[12] A. Prem, S.-J. Huang, H. Song, and M. Hermele, Cage-net fracton models, *Phys. Rev. X* **9**, 021010 (2019).

[13] Y.-T. Hu, M.-Y. Li, and P. Ye, Preparing code states via seed-entangler-enriched sequential quantum circuits: Application to tetradigit topological error-correcting codes, *Phys. Rev. B* **112**, 165139 (2025).

[14] M.-Y. Li and P. Ye, Fracton physics of spatially extended excitations, *Phys. Rev. B* **101**, 245134 (2020).

[15] M.-Y. Li and P. Ye, Fracton physics of spatially extended excitations. ii. polynomial ground state degeneracy of exactly solvable models, *Phys. Rev. B* **104**, 235127 (2021).

[16] M.-Y. Li and P. Ye, Hierarchy of entanglement renormalization and long-range entangled states, *Phys. Rev. B* **107**, 115169 (2023).

[17] K. Slagle, Foliated quantum field theory of fracton order, *Phys. Rev. Lett.* **126**, 101603 (2021).

[18] C. Zhou, M.-Y. Li, Z. Yan, P. Ye, and Z. Y. Meng, Evolution of dynamical signature in the x-cube fracton topological order, *Phys. Rev. Res.* **4**, 033111 (2022).

[19] G.-Y. Zhu, J.-Y. Chen, P. Ye, and S. Trebst, Topological fracton quantum phase transitions by tuning exact tensor network states, *Phys. Rev. Lett.* **130**, 216704 (2023).

[20] G. Canossa, L. Pollet, M. A. Martin-Delgado, H. Song, and K. Liu, Exotic symmetry breaking properties of self-dual fracton spin models, *Phys. Rev. Res.* **6**, 013304 (2024).

[21] T. Devakul, S. A. Parameswaran, and S. L. Sondhi, Correlation function diagnostics for type-i fracton phases, *Phys. Rev. B* **97**, 041110 (2018).

[22] Y. You, T. Devakul, F. J. Burnell, and S. L. Sondhi, Subsystem symmetry protected topological order, *Phys. Rev. B* **98**, 035112 (2018).

[23] Y. You, T. Devakul, S. L. Sondhi, and F. J. Burnell, Fractonic chern-simons and bf theories, *Phys. Rev. Res.* **2**, 023249 (2020).

[24] D. T. Stephen, H. P. Nautrup, J. Bermejo-Vega, J. Eisert, and R. Raussendorf, Subsystem symmetries, quantum cellular automata, and computational phases of quantum matter, *Quantum* **3**, 142 (2019).

[25] A. T. Schmitz, S.-J. Huang, and A. Prem, Entanglement spectra of stabilizer codes: A window into gapped quantum phases of matter, *Phys. Rev. B* **99**, 205109 (2019).

[26] J. F. San Miguel, A. Dua, and D. J. Williamson, Bifurcating subsystem symmetric entanglement renormalization in two dimensions, *Phys. Rev. B* **103**, 035148 (2021).

[27] T. Devakul, Y. You, F. J. Burnell, and S. L. Sondhi, Fractal Symmetric Phases of Matter, *SciPost Phys.* **6**, 007 (2019).

[28] T. Devakul and D. J. Williamson, Universal quantum computation using fractal symmetry-protected cluster phases, *Phys. Rev. A* **98**, 022332 (2018).

[29] T. Devakul, Classifying local fractal subsystem symmetry-protected topological phases, *Phys. Rev. B* **99**, 235131 (2019).

[30] F. J. Burnell, T. Devakul, P. Gorantla, H. T. Lam, and S.-H. Shao, Anomaly inflow for subsystem symmetries, *Phys. Rev. B* **106**, 085113 (2022).

[31] J.-Y. Zhang and P. Ye, Programmable anyon mobility through higher order cellular automata, arXiv preprint arXiv:2508.13961 (2025).

[32] C. Zhou, M.-Y. Li, Z. Yan, P. Ye, and Z. Y. Meng, Detecting subsystem symmetry protected topological order through strange correlators, *Phys. Rev. B* **106**, 214428 (2022).

[33] J.-Y. Zhang, M.-Y. Li, and P. Ye, Higher-order cellular automata generated symmetry-protected topological phases and detection through multi point strange correlators, *PRX Quantum* **5**, 030342 (2024).

[34] M. Pretko, Generalized electromagnetism of subdimensional particles: A spin liquid story, *Phys. Rev. B* **96**, 035119 (2017).

[35] M. Pretko, Subdimensional particle structure of higher rank $u(1)$ spin liquids, *Phys. Rev. B* **95**, 115139 (2017).

[36] M. Pretko, The fracton gauge principle, *Phys. Rev. B* **98**, 115134 (2018).

[37] S. Pai and M. Pretko, Dynamical scar states in driven fracton systems, *Phys. Rev. Lett.* **123**, 136401 (2019).

[38] H. Ma and M. Pretko, Higher-rank deconfined quantum criticality at the lifshitz transition and the exciton bose condensate, *Phys. Rev. B* **98**, 125105 (2018).

[39] S. Pai and M. Pretko, Fractonic line excitations: An inroad from three-dimensional elasticity theory, *Phys. Rev. B* **97**, 235102 (2018).

[40] S. Pai, M. Pretko, and R. M. Nandkishore, Localization

in fractonic random circuits, *Phys. Rev. X* **9**, 021003 (2019).

[41] A. Gromov, Towards classification of fracton phases: The multipole algebra, *Phys. Rev. X* **9**, 031035 (2019).

[42] J. Wang and S.-T. Yau, Non-abelian gauged fracton matter field theory: Sigma models, superfluids, and vortices, *Phys. Rev. Res.* **2**, 043219 (2020).

[43] A. Gromov, A. Lucas, and R. M. Nandkishore, Fracton hydrodynamics, *Phys. Rev. Res.* **2**, 033124 (2020).

[44] J. Feldmeier, P. Sala, G. De Tomasi, F. Pollmann, and M. Knap, Anomalous diffusion in dipole- and higher-moment-conserving systems, *Phys. Rev. Lett.* **125**, 245303 (2020).

[45] J.-K. Yuan, S. A. Chen, and P. Ye, Fractonic superfluids, *Phys. Rev. Res.* **2**, 023267 (2020).

[46] S. A. Chen, J.-K. Yuan, and P. Ye, Fractonic superfluids. ii. condensing subdimensional particles, *Phys. Rev. Res.* **3**, 013226 (2021).

[47] H.-X. Wang, S. A. Chen, and P. Ye, Fractonic superfluids. iii. hybridizing higher moments, *Phys. Rev. Res.* **7**, 033118 (2025).

[48] J.-K. Yuan, S. A. Chen, and P. Ye, Quantum hydrodynamics of fractonic superfluids with lineon condensate: From navier–stokes-like equations to landau-like criterion, *Chin. Phys. Lett.* **39**, 057101 (2022).

[49] H. Li and P. Ye, Renormalization group analysis on emergence of higher rank symmetry and higher moment conservation, *Phys. Rev. Res.* **3**, 043176 (2021).

[50] J.-K. Yuan, S. A. Chen, and P. Ye, Hierarchical proliferation of higher-rank symmetry defects in fractonic superfluids, *Phys. Rev. B* **107**, 205134 (2023).

[51] S. A. Chen and P. Ye, Many-body physics of spontaneously broken higher-rank symmetry: from fractonic superfluids to dipolar hubbard model (2023), arXiv:2305.00941 [cond-mat.str-el].

[52] D. Doshi and A. Gromov, Vortices as fractons, *Communications Physics* **4**, 44 (2021).

[53] K. T. Grosvenor, C. Hoyos, F. Peña Benítez, and P. Surówka, Hydrodynamics of ideal fracton fluids, *Phys. Rev. Res.* **3**, 043186 (2021).

[54] J. Wang, K. Xu, and S.-T. Yau, Higher-rank tensor non-abelian field theory: Higher-moment or subdimensional polynomial global symmetry, algebraic variety, noether's theorem, and gauging, *Phys. Rev. Res.* **3**, 013185 (2021).

[55] R. Argurio, C. Hoyos, D. Musso, and D. Naegels, Fractons in effective field theories for spontaneously broken translations, *Phys. Rev. D* **104**, 105001 (2021).

[56] J. Iaconis, A. Lucas, and R. Nandkishore, Multipole conservation laws and subdiffusion in any dimension, *Phys. Rev. E* **103**, 022142 (2021).

[57] C. Stahl, E. Lake, and R. Nandkishore, Spontaneous breaking of multipole symmetries, *Phys. Rev. B* **105**, 155107 (2022).

[58] L. Radzhivsky, Lifshitz gauge duality, *Phys. Rev. B* **106**, 224510 (2022).

[59] A. Osborne and A. Lucas, Infinite families of fracton fluids with momentum conservation, *Phys. Rev. B* **105**, 024311 (2022).

[60] A. Kapustin and L. Spodyneiko, Hohenberg-mermin-wagner-type theorems and dipole symmetry, *Phys. Rev. B* **106**, 245125 (2022).

[61] E. Lake, M. Hermele, and T. Senthil, Dipolar bose-hubbard model, *Phys. Rev. B* **106**, 064511 (2022).

[62] E. Lake, H.-Y. Lee, J. H. Han, and T. Senthil, Dipole condensates in tilted bose-hubbard chains, *Phys. Rev. B* **107**, 195132 (2023).

[63] K. Giergiel, R. Lier, P. Surówka, and A. Kosior, Bose-hubbard realization of fracton defects, *Phys. Rev. Res.* **4**, 023151 (2022).

[64] P. Zechmann, E. Altman, M. Knap, and J. Feldmeier, Fractonic luttinger liquids and supersolids in a constrained bose-hubbard model, *Phys. Rev. B* **107**, 195131 (2023).

[65] J. Boesl, P. Zechmann, J. Feldmeier, and M. Knap, Deconfinement dynamics of fractons in tilted bose-hubbard chains, *Phys. Rev. Lett.* **132**, 143401 (2024).

[66] W. Xu, C. Lv, and Q. Zhou, Multipolar condensates and multipolar Josephson effects, *Nature Communications* **15**, 4786 (2024).

[67] P. Gorantla, H. T. Lam, N. Seiberg, and S.-H. Shao, Global dipole symmetry, compact lifshitz theory, tensor gauge theory, and fractons, *Phys. Rev. B* **106**, 045112 (2022).

[68] K. T. Grosvenor, C. Hoyos, F. Peña-Benítez, and P. Surówka, Space-dependent symmetries and fractons, *Frontiers in Physics* **9**, 10.3389/fphy.2021.792621 (2022).

[69] E. Lake and T. Senthil, Non-fermi liquids from kinetic constraints in tilted optical lattices, *Phys. Rev. Lett.* **131**, 043403 (2023).

[70] J. Molina-Vilaplana, A post-Gaussian approach to dipole symmetries and interacting fractons, *Journal of High Energy Physics* **2023**, 65 (2023).

[71] P. Gorantla, H. T. Lam, N. Seiberg, and S.-H. Shao, (2+1)-dimensional compact lifshitz theory, tensor gauge theory, and fractons, *Phys. Rev. B* **108**, 075106 (2023).

[72] A. Anakru and Z. Bi, Non-fermi liquids from dipolar symmetry breaking, *Phys. Rev. B* **108**, 165112 (2023).

[73] P. Glorioso, X. Huang, J. Guo, J. F. Rodriguez-Nieva, and A. Lucas, Goldstone bosons and fluctuating hydrodynamics with dipole and momentum conservation, *Journal of High Energy Physics* **2023**, 22 (2023).

[74] A. Morningstar, N. O'Dea, and J. Richter, Hydrodynamics in long-range interacting systems with center-of-mass conservation, *Phys. Rev. B* **108**, L020304 (2023).

[75] X. Huang, A Chern-Simons theory for dipole symmetry, *SciPost Phys.* **15**, 153 (2023).

[76] E. Afxonidis, A. Caddeo, C. Hoyos, and D. Musso, Dipole symmetry breaking and fractonic Nambu-Goldstone mode, *SciPost Phys. Core* **6**, 082 (2023).

[77] C. Stahl, M. Qi, P. Glorioso, A. Lucas, and R. Nandkishore, Fracton superfluid hydrodynamics, *Phys. Rev. B* **108**, 144509 (2023).

[78] H. T. Lam, Classification of dipolar symmetry-protected topological phases: Matrix product states, stabilizer hamiltonians, and finite tensor gauge theories, *Phys. Rev. B* **109**, 115142 (2024).

[79] J. H. Han, E. Lake, and S. Ro, Scaling and localization in multipole-conserving diffusion, *Phys. Rev. Lett.* **132**, 137102 (2024).

[80] F. J. Burnell, S. Moudgalya, and A. Prem, Filling constraints on translation invariant dipole conserving systems, *Phys. Rev. B* **110**, L121113 (2024).

[81] A. Chavda, D. Naegels, and J. Staunton, Fractonic coset construction for spontaneously broken translations, *Phys. Rev. D* **111**, 085018 (2025).

[82] J. Armas and E. Have, Ideal fracton superfluids, *SciPost*

<https://doi.org/10.1142/S0217979292000037>.

[122] A. Lopez and E. Fradkin, Fractional quantum hall effect and chern-simons gauge theories, *Phys. Rev. B* **44**, 5246 (1991).

[123] P. Ye, T. L. Hughes, J. Maciejko, and E. Fradkin, Composite particle theory of three-dimensional gapped fermionic phases: Fractional topological insulators and charge-loop excitation symmetry, *Phys. Rev. B* **94**, 115104 (2016).

[124] R. M. Gray, Toeplitz and circulant matrices: A review, *Foundations and Trends® in Communications and Information Theory* **2**, 155 (2006).

[125] X.-L. Qi and S.-C. Zhang, Topological insulators and superconductors, *Rev. Mod. Phys.* **83**, 1057 (2011).

[126] G. T. Horowitz and M. Srednicki, A quantum field theoretic description of linking numbers and their generalization, *Commun. Math. Phys.* **130**, 83 (1990).

[127] T. Hansson, V. Oganesyan, and S. Sondhi, Superconductors are topologically ordered, *Annals of Physics* **313**, 497 (2004).

[128] B. Moy, H. Goldman, R. Sohal, and E. Fradkin, Theory of oblique topological insulators, *SciPost Phys.* **14**, 023 (2023).

[129] P. Ye and X.-G. Wen, Constructing symmetric topological phases of bosons in three dimensions via fermionic projective construction and dyon condensation, *Phys. Rev. B* **89**, 045127 (2014).

[130] P. Putrov, J. Wang, and S.-T. Yau, Braiding statistics and link invariants of bosonic/fermionic topological quantum matter in 2+1 and 3+1 dimensions, *Annals of Physics* **384**, 254 (2017).

[131] Q.-R. Wang, M. Cheng, C. Wang, and Z.-C. Gu, Topological quantum field theory for abelian topological phases and loop braiding statistics in (3+1)-dimensions, *Phys. Rev. B* **99**, 235137 (2019).

[132] P. Ye and Z.-C. Gu, Topological quantum field theory of three-dimensional bosonic abelian-symmetry-protected topological phases, *Phys. Rev. B* **93**, 205157 (2016).

[133] X. Wen, H. He, A. Tiwari, Y. Zheng, and P. Ye, Entanglement entropy for (3+1)-dimensional topological order with excitations, *Phys. Rev. B* **97**, 085147 (2018).

[134] A. P. O. Chan, P. Ye, and S. Ryu, Braiding with borromean rings in (3+1)-dimensional spacetime, *Phys. Rev. Lett.* **121**, 061601 (2018).

[135] Z.-F. Zhang and P. Ye, Compatible braidings with Hopf links, multi-loop, and Borromean rings in (3+1)-dimensional spacetime, *Phys. Rev. Research* **3**, 023132 (2021).

[136] P. Ye and Z.-C. Gu, Vortex-line condensation in three dimensions: A physical mechanism for bosonic topological insulators, *Phys. Rev. X* **5**, 021029 (2015).

[137] P. Ye and J. Wang, Symmetry-protected topological phases with charge and spin symmetries: Response theory and dynamical gauge theory in two and three dimensions, *Phys. Rev. B* **88**, 235109 (2013).

[138] J. Preskill and L. M. Krauss, Local discrete symmetry and quantum-mechanical hair, *Nuclear Physics B* **341**, 50 (1990).

[139] M. G. Alford and F. Wilczek, Aharonov-bohm interaction of cosmic strings with matter, *Phys. Rev. Lett.* **62**, 1071 (1989).

[140] L. M. Krauss and F. Wilczek, Discrete gauge symmetry in continuum theories, *Phys. Rev. Lett.* **62**, 1221 (1989).

[141] M. G. Alford, K.-M. Lee, J. March-Russell, and J. Preskill, Quantum field theory of non-abelian strings and vortices, *Nuclear Physics B* **384**, 251 (1992).

[142] C. Wang and M. Levin, Braiding statistics of loop excitations in three dimensions, *Phys. Rev. Lett.* **113**, 080403 (2014).

[143] J. C. Wang, Z.-C. Gu, and X.-G. Wen, Field-theory representation of gauge-gravity symmetry-protected topological invariants, group cohomology, and beyond, *Phys. Rev. Lett.* **114**, 031601 (2015).

[144] J. C. Wang and X.-G. Wen, Non-abelian string and particle braiding in topological order: Modular $SL(3, \mathbb{Z})$ representation and (3+1)-dimensional twisted gauge theory, *Phys. Rev. B* **91**, 035134 (2015).

[145] C.-M. Jian and X.-L. Qi, Layer construction of 3d topological states and string braiding statistics, *Phys. Rev. X* **4**, 041043 (2014).

[146] S. Jiang, A. Mesaros, and Y. Ran, Generalized modular transformations in (3+1)D topologically ordered phases and triple linking invariant of loop braiding, *Phys. Rev. X* **4**, 031048 (2014).

[147] C. Wang, C.-H. Lin, and M. Levin, Bulk-boundary correspondence for three-dimensional symmetry-protected topological phases, *Phys. Rev. X* **6**, 021015 (2016).

[148] A. Tiwari, X. Chen, and S. Ryu, Wilson operator algebras and ground states of coupled BF theories, *Phys. Rev. B* **95**, 245124 (2017).

[149] A. Kapustin and R. Thorngren, Anomalies of discrete symmetries in various dimensions and group cohomology, ArXiv e-prints (2014), arXiv:1404.3230 [hep-th].

[150] Y. Wan, J. C. Wang, and H. He, Twisted gauge theory model of topological phases in three dimensions, *Phys. Rev. B* **92**, 045101 (2015).

[151] X. Chen, A. Tiwari, and S. Ryu, Bulk-boundary correspondence in (3+1)-dimensional topological phases, *Phys. Rev. B* **94**, 045113 (2016).

[152] A. Kapustin and N. Seiberg, Coupling a QFT to a TQFT and Duality, *JHEP* **04**, 001, arXiv:1401.0740 [hep-th].

[153] Z.-F. Zhang, Q.-R. Wang, and P. Ye, Continuum field theory of three-dimensional topological orders with emergent fermions and braiding statistics, *Phys. Rev. Res.* **5**, 043111 (2023).

[154] X.-L. Qi and S.-C. Zhang, Topological insulators and superconductors, *Rev. Mod. Phys.* **83**, 1057 (2011).

[155] M. F. Lapa, C.-M. Jian, P. Ye, and T. L. Hughes, Topological electromagnetic responses of bosonic quantum hall, topological insulator, and chiral semimetal phases in all dimensions, *Phys. Rev. B* **95**, 035149 (2017).

[156] P. Ye, M. Cheng, and E. Fradkin, Fractional s -duality, classification of fractional topological insulators, and surface topological order, *Phys. Rev. B* **96**, 085125 (2017).

[157] E. Witten, Fermion path integrals and topological phases, *Rev. Mod. Phys.* **88**, 035001 (2016).

[158] B. Han, H. Wang, and P. Ye, Generalized wen-zee terms, *Phys. Rev. B* **99**, 205120 (2019).

[159] S.-Q. Ning, Z.-X. Liu, and P. Ye, Fractionalizing global symmetry on looplike topological excitations, *Phys. Rev. B* **105**, 205137 (2022).

[160] S.-Q. Ning, Z.-X. Liu, and P. Ye, Symmetry enrichment in three-dimensional topological phases, *Phys. Rev. B* **94**, 245120 (2016).

[161] P. Ye, Three-dimensional anomalous twisted gauge theories with global symmetry: Implications for quantum

spin liquids, *Phys. Rev. B* **97**, 125127 (2018).

[162] Z.-F. Zhang, Q.-R. Wang, and P. Ye, Non-abelian fusion, shrinking, and quantum dimensions of abelian gauge fluxes, *Phys. Rev. B* **107**, 165117 (2023).

[163] Y. Huang, Z.-F. Zhang, and P. Ye, Fusion rules and shrinking rules of topological orders in five dimensions, *Journal of High Energy Physics* **2023**, 210 (2023), arXiv:2306.14611 [hep-th].

[164] Y. Huang, Z.-F. Zhang, and P. Ye, Diagrammatics, pentagon equations, and hexagon equations of topological orders with loop- and membrane-like excitations, *Journal of High Energy Physics* **2025**, 238 (2025), arXiv:2405.19077 [hep-th].

[165] N. Hatano and D. R. Nelson, Localization transitions in non-hermitian quantum mechanics, *Phys. Rev. Lett.* **77**, 570 (1996).

[166] B. Zhu, R. Lü, and S. Chen, \mathcal{PT} symmetry in the non-hermitian su-schrieffer-heeger model with complex boundary potentials, *Phys. Rev. A* **89**, 062102 (2014).

[167] S. Lieu, Topological phases in the non-hermitian su-schrieffer-heeger model, *Phys. Rev. B* **97**, 045106 (2018).

[168] R. A. Horn and C. R. Johnson, *Matrix analysis* (Cambridge university press, 2012).

[169] D. Porras and S. Fernández-Lorenzo, Topological amplification in photonic lattices, *Phys. Rev. Lett.* **122**, 143901 (2019).

[170] T. Ramos, J. J. Garcia-Ripoll, and D. Porras, Topological input-output theory for directional amplification, *Phys. Rev. A* **103**, 033513 (2021).

[171] M. Brunelli, C. C. Wanjura, and A. Nunnenkamp, Restoration of the non-Hermitian bulk-boundary correspondence via topological amplification, *SciPost Phys.* **15**, 173 (2023).

[172] W.-T. Xue, M.-R. Li, Y.-M. Hu, F. Song, and Z. Wang, Simple formulas of directional amplification from non-bloch band theory, *Phys. Rev. B* **103**, L241408 (2021).

[173] D. S. Dummit, R. M. Foote, *et al.*, *Abstract algebra*, Vol. 3 (Wiley Hoboken, 2004).

[174] G. H. Golub and C. F. Van Loan, *Matrix computations* (JHU press, 2013).

[175] V. M. Martinez Alvarez, J. E. Barrios Vargas, and L. E. F. Foa Torres, Non-Hermitian robust edge states in one dimension: Anomalous localization and eigenspace condensation at exceptional points, *Phys. Rev. B* **97**, 121401 (2018), arXiv:1711.05235 [cond-mat.mes-hall].

[176] S. Yao and Z. Wang, Edge States and Topological Invariants of Non-Hermitian Systems, *Phys. Rev. Lett.* **121**, 086803 (2018).

[177] K. Yokomizo and S. Murakami, Non-Bloch Band Theory of Non-Hermitian Systems, *Phys. Rev. Lett.* **123**, 066404 (2019).

[178] S. Weidemann, M. Kremer, T. Helbig, T. Hofmann, A. Stegmaier, M. Greiter, R. Thomale, and A. Szameit, Topological funneling of light, *Science* **368**, 311 (2020), <https://www.science.org/doi/pdf/10.1126/science.aaz8727>.

[179] L. Xiao, T. Deng, K. Wang, G. Zhu, Z. Wang, W. Yi, and P. Xue, Non-Hermitian bulk-boundary correspondence in quantum dynamics, *Nature Physics* **16**, 761 (2020), arXiv:1907.12566 [cond-mat.mes-hall].

[180] T. Helbig, T. Hofmann, S. Imhof, M. Abdelghany, T. Kiessling, L. W. Molenkamp, C. H. Lee, A. Szameit, M. Greiter, and R. Thomale, Generalized bulk-boundary correspondence in non-Hermitian topoelectrical circuits, *Nat. Phys.* **16**, 747 (2020).

[181] K. Zhang, Z. Yang, and C. Fang, Correspondence between Winding Numbers and Skin Modes in Non-Hermitian Systems, *Phys. Rev. Lett.* **125**, 126402 (2020).

[182] X. Zhang, Y. Tian, J.-H. Jiang, M.-H. Lu, and Y.-F. Chen, Observation of higher-order non-Hermitian skin effect, *Nature Communications* **12**, 5377 (2021), arXiv:2102.09825 [physics.app-ph].

[183] Q. Liang, D. Xie, Z. Dong, H. Li, H. Li, B. Gadway, W. Yi, and B. Yan, Dynamic Signatures of Non-Hermitian Skin Effect and Topology in Ultracold Atoms, *Phys. Rev. Lett.* **129**, 070401 (2022), arXiv:2201.09478 [cond-mat.quant-gas].

[184] K. Zhang, Z. Yang, and C. Fang, Universal non-Hermitian skin effect in two and higher dimensions, *Nat Commun* **13**, 2496 (2022).

[185] E. Zhao, Z. Wang, C. He, T. F. J. Poon, K. K. Pak, Y.-J. Liu, P. Ren, X.-J. Liu, and G.-B. Jo, Two-dimensional non-Hermitian skin effect in an ultracold Fermi gas, *Nature (London)* **637**, 565 (2025), arXiv:2311.07931 [cond-mat.quant-gas].

[186] B. Hetényi and B. Dóra, Localized states and skin effect around non-Hermitian impurities in tight-binding models, *Phys. Rev. B* **112**, 075123 (2025), arXiv:2508.00519 [cond-mat.mes-hall].

[187] W. P. Su, J. R. Schrieffer, and A. J. Heeger, Soliton excitations in polyacetylene, *Phys. Rev. B* **22**, 2099 (1980).

[188] F. A. Wolf, *Parallel universes* (Simon and Schuster, 1990).

[189] M. S. Morris, K. S. Thorne, and U. Yurtsever, Wormholes, time machines, and the weak energy condition, *Phys. Rev. Lett.* **61**, 1446 (1988).

[190] Y. Huang, Z.-F. Zhang, Q.-R. Wang, and P. Ye, Bridging Microscopic Constructions and Continuum Topological Field Theory of Three-Dimensional Non-Abelian Topological Order, *arXiv e-prints*, arXiv:2512.21148 (2025), arXiv:2512.21148 [cond-mat.str-el].

[191] Z.-F. Zhang, Y. Huang, Q.-R. Wang, and P. Ye, Field-Theoretical Construction of Conserved Currents, Non-Invertible Symmetries, and Mixed Anomalies in Three-Dimensional Non-Abelian Topological Order, *arXiv e-prints*, arXiv:2601.01523 (2026), arXiv:2601.01523 [cond-mat.str-el].